Engineering Silica Membranes for Separation Performance, Hydrothermal Stability, and Production Scalability

Vinh Bui, Ameya Manoj Tandel, Varun Reddy Satti, Elizabeth Haddad, and Haiqing Lin*

Department of Chemical and Biological Engineering, University at Buffalo, The State University of New York, Buffalo, NY 14260, USA

* Corresponding author: Haiqing Lin, e-mail: haiqingl@buffalo.edu

Prepared for submission to *Advanced Membranes*

Abstract

Silica membranes have been successfully practiced for solvent dehydration and emerged as an exciting platform for gas separations (such as H_2/CO_2) due to their unique porous structures for molecular sieving, tunable chemistries, and excellent thermal and chemical stability. This review aims to provide a comprehensive update on the advancement of silica membranes for gas and liquid separations in the last decade. First, we summarize various techniques to fabricate membranes (particularly those at low temperatures) and describe the effect of processing parameters on the membrane structures. Second, penetrant transport mechanisms and molecular dynamic simulations are presented to elucidate the structure-properties relationship. Third, we highlight state-of-the-art silica membranes with promising separation properties for gases, vapors, and liquids and various engineering strategies to improve hydrothermal stability, production scalability, and separation performance. Finally, we provide perspectives on the future development of these membranes for practical applications.

Keywords: Silica membranes; carbon capture; organosilica membranes; hydrothermal stability; H_2/CO_2 separation; scalability

1. Introduction

Membrane technology has emerged as a leading separation process because of its high energy efficiency, easiness in scale-up and operation, and absence of chemical wastes [1, 2]. For example, membranes have been practiced to desalinate salty water, remove CO_2 from natural gas (CO_2/CH_4 separation), produce N_2 from the air (O_2/N_2 separation), and recover H_2 from dilute streams (H_2/N_2 and H_2/CH_4 separations) [3]. Furthermore, membranes show promise for important applications to enable a low-carbon economy, such as pre-combustion carbon capture (H_2/CO_2 separation) [4-6], post-combustion carbon capture (CO_2/N_2 separation) [7, 8], olefin/paraffin separations, and organic liquid separations [9, 10].

The rapid advancement of membrane technology relies on developing membrane materials with superior separation properties, excellent processability for large-scale production, and stability under practical conditions for long-term operation. Industrial membranes are dominated by polymers due to their low cost and excellent processability [2, 3]. However, polymers usually have random free volume distributions influenced by chemical structures and processing history, leading to a permeability/selectivity tradeoff, i.e., polymers with high gas permeability tend to exhibit weak size-sieving ability [1, 11]. Additionally, polymers do not have chemical and thermal stability as good as inorganic materials.

Silica membranes have attracted significant interest because of their unique porous structures, superior separation properties, and excellent stability against chemicals and high temperatures [12-21]. They have been successfully developed for industrial applications, such as dehydration of solvents by pervaporation [22-29] and membrane reactors [30-32]. Additionally, silica membranes have demonstrated their potential for a wide range of applications, such as hydrogen purification [14, 33], helium recovery [34], olefin/paraffin separation [35], post-

combustion CO_2 capture [36], and desalination [29, 37]. For instance, silica membranes prepared from tetraethyl orthosilicate (TEOS) exhibited H_2 permeance of 1490 GPU (1 GPU = 10^{-6} cm^3(STP) cm^{-2} s^{-1} $cmHg^{-1}$ = 3.35×10^{-10} mol m^{-2} s^{-1} Pa^{-1}) and H_2/CO_2 selectivity of 71 at 200 °C [38], which is highly desirable for H_2 purification [39]. However, their population for industrial applications is restrained by the following challenges: (1) weak hydrothermal stability, where silica networks undergo hydrolysis and densification, decreasing gas permeance and even selectivity [17, 40-42], (2) poor control of pore size and defectivity for robust separations, and (3) high cost and intensive energy consumption for large scale membrane fabrication [14, 43, 44].

Various aspects of silica membrane development have been reviewed, such as chemical vapor deposition (CVD) to prepare membranes for H_2 purification [33], metal ion doping for membrane reactors [45], hydro-stable silica membranes for desalination [46], pervaporation for solvent dehydration and recovery [28], organosilica membranes for gas and liquid separations [29], hybrid silica membranes with organic bridging [47], and amine functionalization for CO_2 separation [36]. However, these reviews often focus on a specific type of silica membranes or a specific application, and the most recent comprehensive review on the development of silica membranes was in 2018 [15], despite the growing interest in the last five years.

This review aims to provide a comprehensive update of silica membranes with fine-tuned molecular size-sieving ability for gas, vapor, and liquid separations, as illustrated in Fig. 1. First, we discuss membrane fabrication techniques (such as sol-gel, CVD, and oxygen-plasma treatment) and the influence of processing parameters on the membrane structures and performance. Second, gas transport mechanisms for silica membranes (including empirical equations and molecular dynamic simulations) are critically reviewed, providing insight into

structure/property relationships. Third, chemical and porous structures of organosilica (organically decorated silica) membranes are summarized, accentuating their advantages in membrane pore size control and hydrothermal enhancement. Fourth, we exhaustively discuss their promising applications and strategies to enhance separation performance, stability, and production scalability. Finally, we present our perspectives on the development and outlook of silica membranes for practical applications.

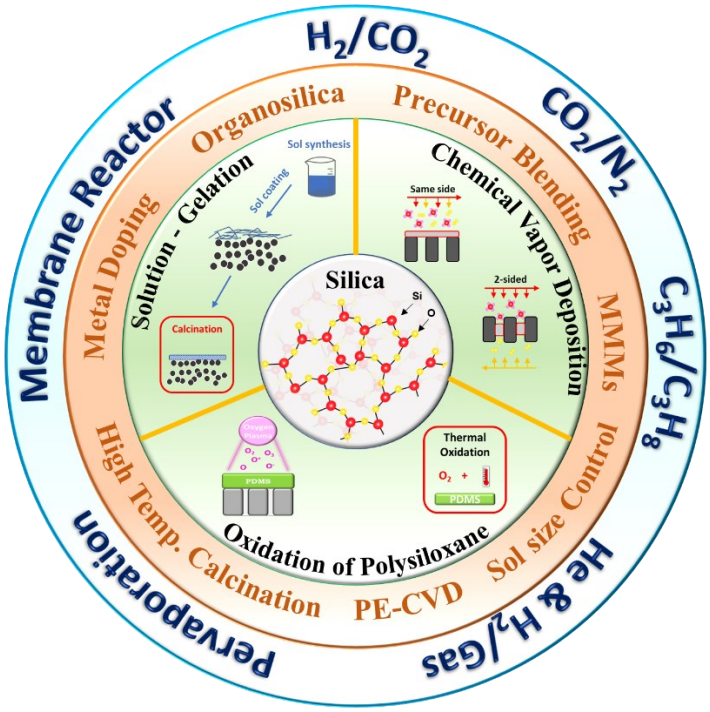

Fig. 1: Overview of silica membranes for molecular separations, including fabrication methods, network engineering, and potential applications.

2. Fabrication techniques for silica membranes

Silica membranes are conventionally fabricated via solution-gelation (sol-gel) or CVD, while new methods operating at room temperature have also been developed, such as plasma-enhanced CVD (PE-CVD) and oxidation of polysiloxanes. This section discusses these methods and the influence of processing parameters on membrane structure and properties.

2.1. Solution-gelation processes

The sol-gel method is the most well-known technique to fabricate silica membranes because of the abundant choices of silica precursors and facile sol modifications to tune separation properties [48]. This technique has three steps: sol preparation, coating, and calcination. The sol is synthesized by simultaneous hydrolysis and polycondensation of alkoxysilanes, as shown below [49, 50]:

$$\equiv Si{-}OR + H_2O \leftrightarrow \equiv Si{-}OH + R{-}OH \quad \text{(R1)}$$

$$\equiv Si{-}OR + \equiv Si{-}OH \leftrightarrow \equiv Si{-}O{-}Si\equiv + R{-}OH \quad \text{(R2)}$$

$$\equiv Si{-}OH + \equiv Si{-}OH \leftrightarrow \equiv Si{-}O{-}Si\equiv + H_2O \quad \text{(R3)}$$

The alkoxides (-OR) are first hydrolyzed to generate silanol (Si-OH) and alcohol groups (Reaction 1), which are then condensed to form Si-O-Si linkages (Reactions 2 and 3). The reactions are often conducted in the presence of an acid or basic catalyst. An acidic catalyst promotes hydrolysis, developing long-chain networks suitable for microporous membranes (with pore sizes less than 2 nm). By contrast, a basic catalyst facilitates condensation, generating highly condensed species and large agglomerates ideal for mesoporous membranes (with pore sizes of 2 – 50 nm) [48-53]. Therefore, the solution composition is essential to optimize the hydrolysis and condensation to fabricate membranes with desirable molecular sieving ability.

To form membranes, the sol is coated onto a porous support followed by calcination at 300 - 700 °C in an inert atmosphere. Various processing parameters can influence the membrane uniformity, mechanical properties, molecular separation properties, and chemical stability, which are presented below.

2.1.1. Sol preparation

Controlling the sol particle size and hydrolysis and condensation degree is the key to fabricating defect-free and molecular-sieving membranes. The sol particles should be large

enough to avoid their penetration into the porous support but not too large to induce voids in the synthesized membranes. On the other hand, increasing the hydrolysis degree increases the silanol content, the Si-O-Si linkages after the calcination, and thus the size-sieving ability.

The sol particle size and its hydrolysis and condensation degree can be manipulated by varying the molar ratios of water to the precursor (WR), acid to the precursor (AR), and solvent to the precursor (SR) in the synthesis solutions [54-58]. Fig. 2 presents an example of the effect of the WR values on the structure and gas separation properties of the membranes derived from triethoxysilane (TRIES) [59]. Increasing the WR value from 6 to 240 increased the sol particle size from 0.7 to 1.0 nm, enabling its coating on supports with pore diameters of 1-2 nm [59]. Higher WR values facilitated hydrolysis of the alkoxyl groups, tightening the silica structures after the calcination (Fig. 2b). Consequently, increasing the WR value from 6 to 240 decreased H_2 permeance from 3000 to 180 GPU and increased H_2/CO_2 from 4.7 (Knudsen selectivity) to 80 [59]. Similarly, increasing the WR value from 2.29 to 5.56 increased the particle size of 1,2-bis(triethoxysiyl)ethane (BTESE) from 3.3 to 5.4 nm [55], and increasing the WR value from 6 to 240 increased H_2/N_2 from 10 to 50 [54].

Increasing the AR value often increases the hydrolysis degree as the acid can catalyze Reaction 1. Nevertheless, in a water-poor environment with low WR values, the sol particle size is independent of the AR, as Reaction 1 is limited by the amount of water [55]. For example, at a WR of 3.44, increasing the AR value from 0.06 to 0.12 in the BTESE sols barely affected the particle size [55], though H_2/CO_2 selectivity decreased from 9.5 to 7.1 and H_2 permeance increased from 870 to 1260 GPU. On the other hand, at a WR of 22.24, increasing the AR from 0.04 to 0.16 increased the particle size from 4 to 9 nm, and a further increase in AR led to bimodal size distribution [55]. Larger sol particles formed larger pores due to insufficient sol

packing and thus decreased the size-sieving ability. For instance, increasing the AR value from 0.01 to 0.1 in BTESE-derived membranes increased H_2 permeance from 564 to 810 GPU and decreased H_2/N_2 selectivity from 50 to 21 [57].

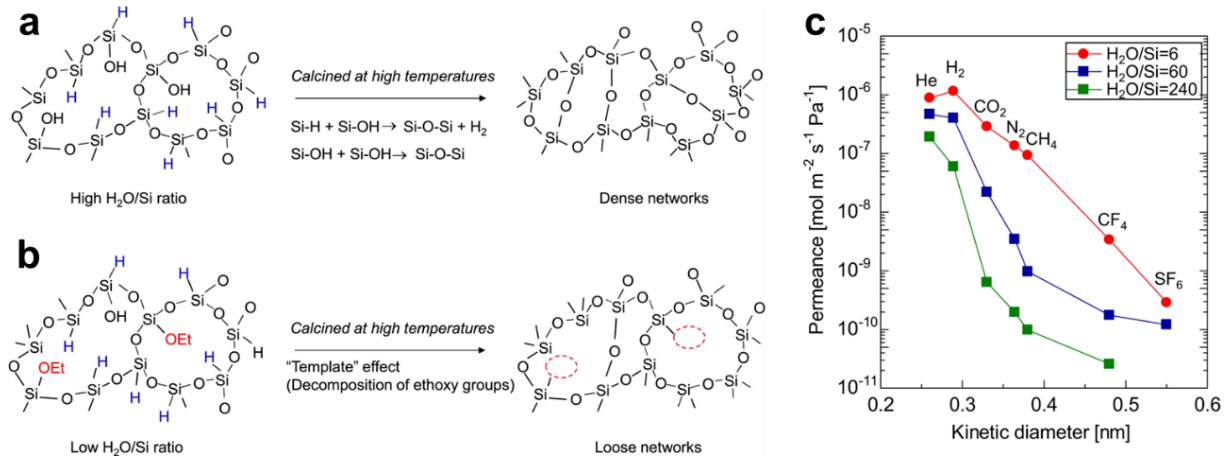

Fig. 2. Effect of the water to precursor molar ratio (WR or H_2O/Si) on the structure and gas transport properties in the TRIES membranes. (a) Dense networks derived from high WR values. (b) Loose networks derived from low WR values. (c) Gas permeance as a function of its kinetic diameter. Copyright (2016) Elsevier [59].

SR is an important parameter to control the solution reactivity and thus the sol particle size. For example, increasing the SR value from 6.54 to 26.16 in BTESE-derived membranes decreased the particle size from 9 to 2 nm because the dilution slowed the sol growth and agglomeration [55]. The solvent polarity and dielectric constant also influenced the sol formation. Fig. 3a presents the schematic of BTESE sol formation in three solvents, N-methyl pyrrolidone (NMP), ethanol (EtOH), and tetrahydrofuran (THF) [60]. In the early stage of sol-gel synthesis, NMP with the highest polarity (6.7) led to a higher degree of hydrolysis than EtOH (4.3) and THF (4.0). However, NMP with the highest dielectric constant of 32.2 weakened the solute-solute interactions and thus slowed the sol growth and agglomeration. Consequently, BTESE sols prepared in NMP had particles of 0.62 nm, much smaller than 2.69 nm for those prepared in EtOH (with a dielectric constant of 24.3) and 3.12 nm for those prepared in THF

(7.6) [60]. The particles were more dispersed and more difficult to polymerize, leading looser networks, higher permeance, and lower selectivity in the NMR-derived membranes (Fig. 3b,c).

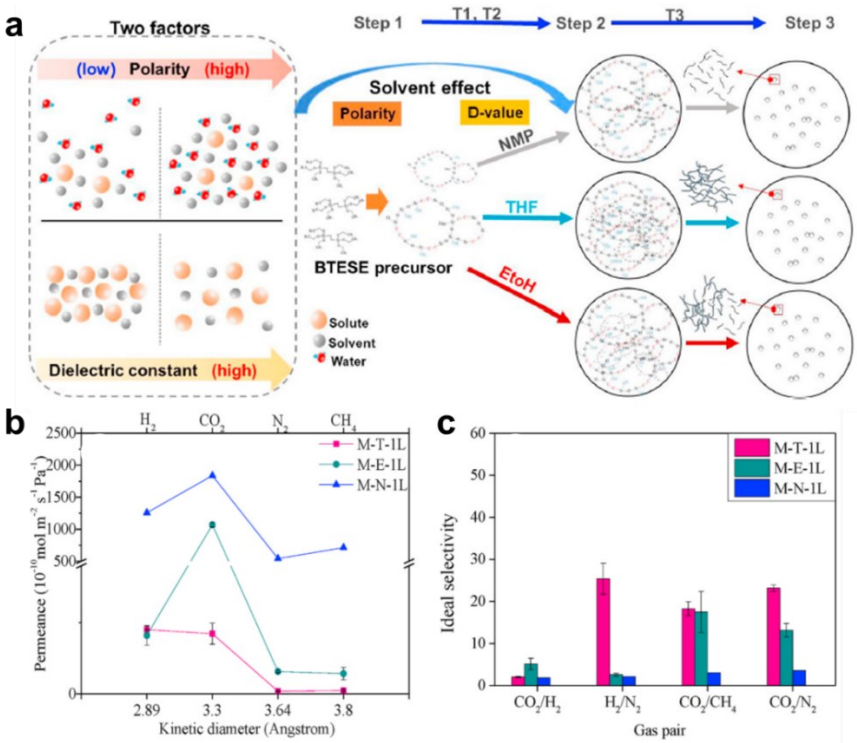

Fig. 3. Effect of the solvent on the structures and gas separation properties of the BTESE-derived organosilica membranes. (a) Structures, (b) pure-gas permeance, and (c) ideal gas selectivity. M-T-IL, M-E-IL, and M-N-IL represent the membranes formed in THF (pink), EtOH (green), and NMP (blue), respectively. Copyright (2020) Elsevier [60].

2.1.2. Sol coating on porous supports

The silica sol can be coated onto porous supports to form membranes using different techniques, such as dip coating, spin coating, flow-induced coating, and spray coating. Spin and dip coating are the commonly used techniques, owing to their simplicity, reliability, and scalability, while flow-induced and spray coating have also been demonstrated for large-scale fabrication. Fig. 4a presents the flow-induced coating technique, where two coatings at different flow directions are used to fabricate membranes. Fig. 4b displays the spray coating of BTESE sol on polysulfone (PSF) porous support.

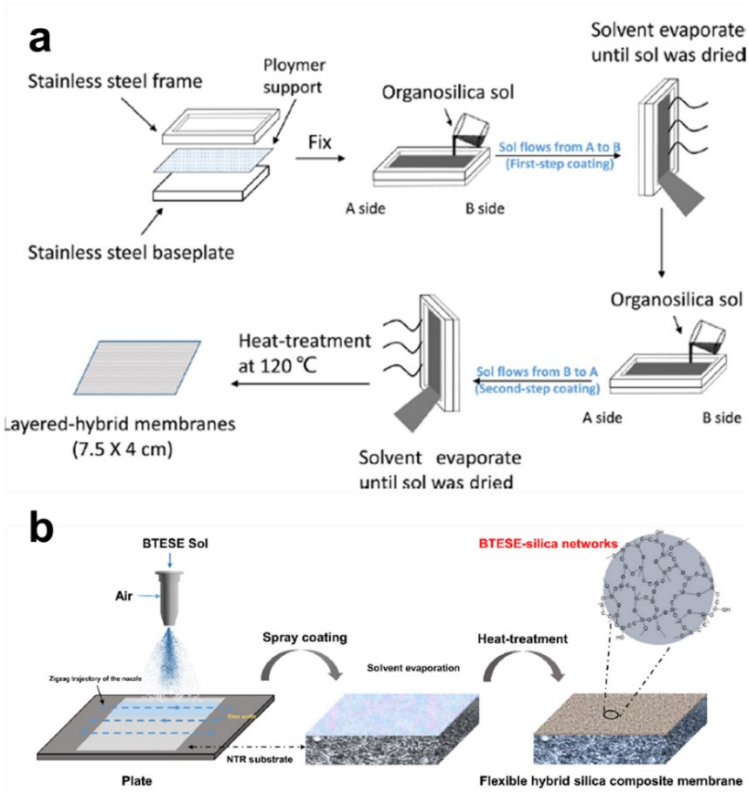

Fig. 4. (a) Membrane coating via flow-induced technique, where two opposite flow directions of the sol solution are applied to produce membranes. Copyright (2018) American Chemical Society [61]. (b) Spray coating of a dilute BTESE solution onto PSF in a zig-zag method. Copyright (2021) Elsevier [44].

The choice of porous supports is critical in forming thin layers with good stability. Conventionally, alumina supports are used due to their robust structure and excellent thermal stability. For example, α-alumina provided mechanical support, while a gutter layer of γ-alumina rendered a smooth surface with uniform pores to coat the selective layer [55, 62]. Alternatively, SiO_2-ZrO_2 was also used as the gutter layer with a pore size of less than 2 nm [63-65]. However, γ-alumina and SiO_2-ZrO_2 are hydrophilic, promoting water condensation in wet conditions, which can block the pores for diffusion and cause hydrothermal instability [66]. To address these issues, a gutter layer with hydrophobic organic groups (such as BTESE and MTMS/TEOS mixtures) was used to reduce water condensation [67, 68]. Nevertheless, these multi-layer substrates require many cycles of coating and calcination at elevated temperatures to achieve

smooth and desirable pore size for defect-free sol coating, and thus they are time-consuming and costly for large-scale fabrication [14, 69].

One strategy to avoid the multicycles of coating and calcination is to use polymeric supports, such as PSF [70, 71] and sulfonated polyethersulfone (SPES) [61, 72]. Similar to sol-coating on inorganic substrates, the silica-sol can form an interlocking structure at the interface with the porous support and thus preventing the silica layer from peeling [73, 74]. In addition, the hydroxyl group on silica sol can form H-bonding with polymeric substrates, which is desirable for an effective coating process. The polymeric substrates can also enhance the overall membrane flexibility and thus handleability. For instance, the BTESE-coated SPES membrane showed stable performance of isopropanol dehydration [73].

2.1.3 Calcination

The sol solutions are often calcinated at 300 - 700 °C to remove volatile components (such as solvents and water) and induce internetwork condensation of silanol groups, tightening the structure and improving molecular sieving properties. Silica membranes are often calcinated in the air, where the presence of oxygen is preferred for network formation. On the other hand, organically decorated membranes are calcinated in N_2 to prevent the degradation of organic groups [75]. Increasing the calcination temperature often tightens the silica structure because of the enhanced silanol condensation and thus densification [76, 77]. For instance, increasing the calcination temperature of TEOS derived membrane from 400 to 600 °C decreased the pore size from < 5.5 to < 3.8 Å [76], and increasing the calcination temperature of BTESE-derived membrane from 300 to 700 °C decreased the BET surface area from 55.8 to 8.0 m^2 g^{-1} and the pore volume from 0.14 to 0.03 cm^3 g^{-1} [77].

2.2. Chemical vapor deposition (CVD)

CVD allows the vapor-phase deposition of thin silica films on top of porous supports via thermal decomposition, hydrolysis, or oxidation of the precursors. Fig. 5 displays a typical CVD schematic, where the precursor is introduced into the reaction chamber using a carrier gas (such as H_2, Ar, or N_2) and reactive species (such as oxygen, air, or water). Because the building blocks in CVD are much smaller than the particles in the sol-gel process, the CVD technique often produces denser silica networks with higher gas selectivity and lower gas permeance. For instance, the Nanosil membrane prepared by CVD of TEOS precursor exhibited H_2 permeance of 540 GPU and H_2/CH_4 selectivity of 4200, while those prepared by sol-gel showed H_2 permeance of 600 GPU and H_2/CH_4 selectivity of only 120 at 600 °C [78, 79].

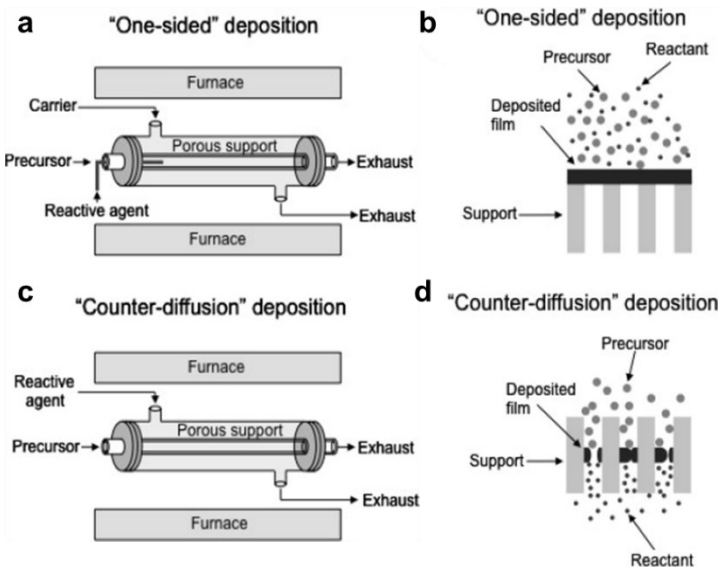

Fig. 5. Schematic of one-sided deposition to form membranes, including (a) the process and (b) the layer formation. Schematic of "counter-diffusion" deposition to form the membranes, including (c) the process and (d) layer formation. Copyright (2013) Elsevier [33].

The silica membranes can be fabricated using different flow configurations for the reactive species and silica precursors. Fig. 5b shows that a one-sided configuration deposits silica films on the substrate surface, while a counter-diffusion mainly deposits silica films on the pore wall. The film formation on the pore wall is often self-limiting because the deposition stops

when the pore neck is smaller than the penetrating species, resulting in a pore diameter approximating the size of the growing species. On the other hand, in the one-sided configuration, the selective layer can continue to grow, lowering gas permeance. For example, dimethyldimethoxysilate (DMDMOS) membranes prepared via the counter-diffusion method showed H_2 permeance of 1300 GPU and N_2 permeance of 1 GPU independent of the deposition times above 60 mins [80]. By contrast, when they were prepared via the one-sided flow with the deposition time increasing from 600 to 900 mins, H_2 permeance decreased from 110 to 75 GPU and N_2 permeance decreased from 6 to 0.3 GPU [81]. In addition to the flow geometry, other processing parameters can influence membrane performance, such as precursor residence time [81], reaction temperature, and deposition pathway [33].

2.3. PE-CVD

The silica membranes prepared by CVD often achieve strong size-sieving ability but low gas permeance, and there are limited choices of precursors because of the high operating temperatures (> 300 °C). To lower the temperature and thus expand the options of precursors, CVD can be coupled with plasma species to accelerate the reaction rate (PE-CVD). In this process, the main gas (such as Ar, O_2, or N_2) is ionized with high-energy plasma and reacts with silica precursors in the vapor phase to deposit on porous supports (Fig. 6a). Various processing parameters can be manipulated to optimize membrane structures, such as the main gas [82, 83], post-synthesis annealing conditions [83], deposition time [82, 84], deposition rate [85], and deposition temperature [86]. For example, hexamethyldisiloxane (HMDSO) was deposited using Ar plasma, and increasing the deposition temperature from 50 to 200 °C lowered carbon content and increased silica-like content and He/SF_6 selectivity from 100 to 1000 [86]. Fig. 6b illustrates

the deposition of HMDSO in the Ar discharge region, achieving a thickness of ≈30 nm due to the balanced organosilica deposition and Ar-plasma etching [86].

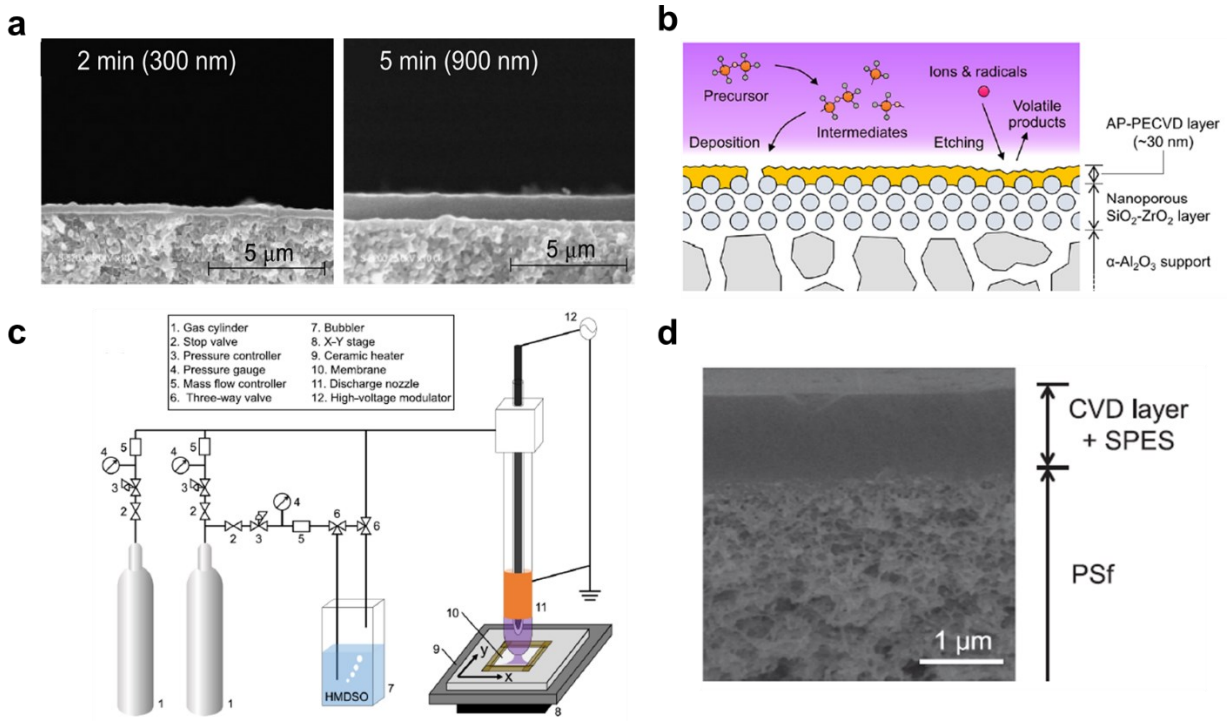

Fig. 6. (a) HDMSO-derived membranes using PE-CVD. Cross-sectional SEM of the membranes with deposition times of 2 and 5 mins. Copyright (2013) Elsevier [82]. (b) Schematic of the balanced effect between the film deposition and Ar-etching on the silica layer (≈30 nm). Copyright (2021) American Chemical Society [86]. (c) Schematic of the open-air PE-CVD and (d) cross-sectional SEM of HDMSO deposited on PSF support using open-air PE-CVD. Copyright (2022) Elsevier [43].

To further demonstrate the applicability of PE-CVD for large-scale fabrication, open-air PE-CVD was employed on porous PSF support [43, 69]. As shown in Fig. 6c, the main gas (Ar/N_2) is bubbled through the HMDSO reservoir to the plasma nozzle and ejected onto the PSF support [43]. Fig. 6d shows the cross-sectional SEM image of an example membrane. The structure and separation properties of the membranes can be influenced by the number of coating cycles and HDMSO concentration in the gas mixture. For example, increasing the HDMSO concentration from 54 to 784 ppm increased the layer thickness from 200 to 800 nm [43];

increasing the coating cycle from 2 to 8 decreased He permeance from 21,000 to 450 GPU and increased He/SF_6 selectivity from 6 to 41 [69].

2.4. Oxidation of polysiloxanes

Oxidation of polysiloxanes via thermal or plasma treatment can be an attractive approach to fabricate silica membranes. First, the excellent film formability of polysiloxanes allows one-step, defect-free coating on porous substrates. Second, the low temperature of plasma treatment allows the use of inexpensive porous substrates [14]. Third, both thermal and plasma processes are readily available in the industry for large-scale fabrication. Fig. 7a presents the oxidation thermolysis of polydimethylsiloxane (PDMS)/TEOS films, where methyl groups are first oxidized to produce hydroxide groups, followed by water condensation of adjacent silanol (Si-OH) groups, resulting in Si-O-Si linkages [87]. Fig. 7b presents the FTIR spectrum of the resultant membranes, confirming the successful synthesis of silica.

Polysiloxanes can also be oxidized by oxygen plasma at room temperature for a short time (e.g., 1-3 mins) to form silica [14]. Fig. 7c presents the conversion of PDMS by oxygen-plasma treatment, where oxygen ions cleave methyl groups to form Si-O-Si linkages. Increasing plasma exposure time increased the silica-like content on the membrane surface, as evidenced by the increased O/Si ratio and decreased C/Si ratio (Fig. 7d). Furthermore, Fig. 7e presents that the O/Si ratio decreased along the membrane thickness, suggesting a gradual change from the silica (with the O/Si ratio of 2) on the surface to PDMS (with the O/Si ratio of 1) in bulk [14].

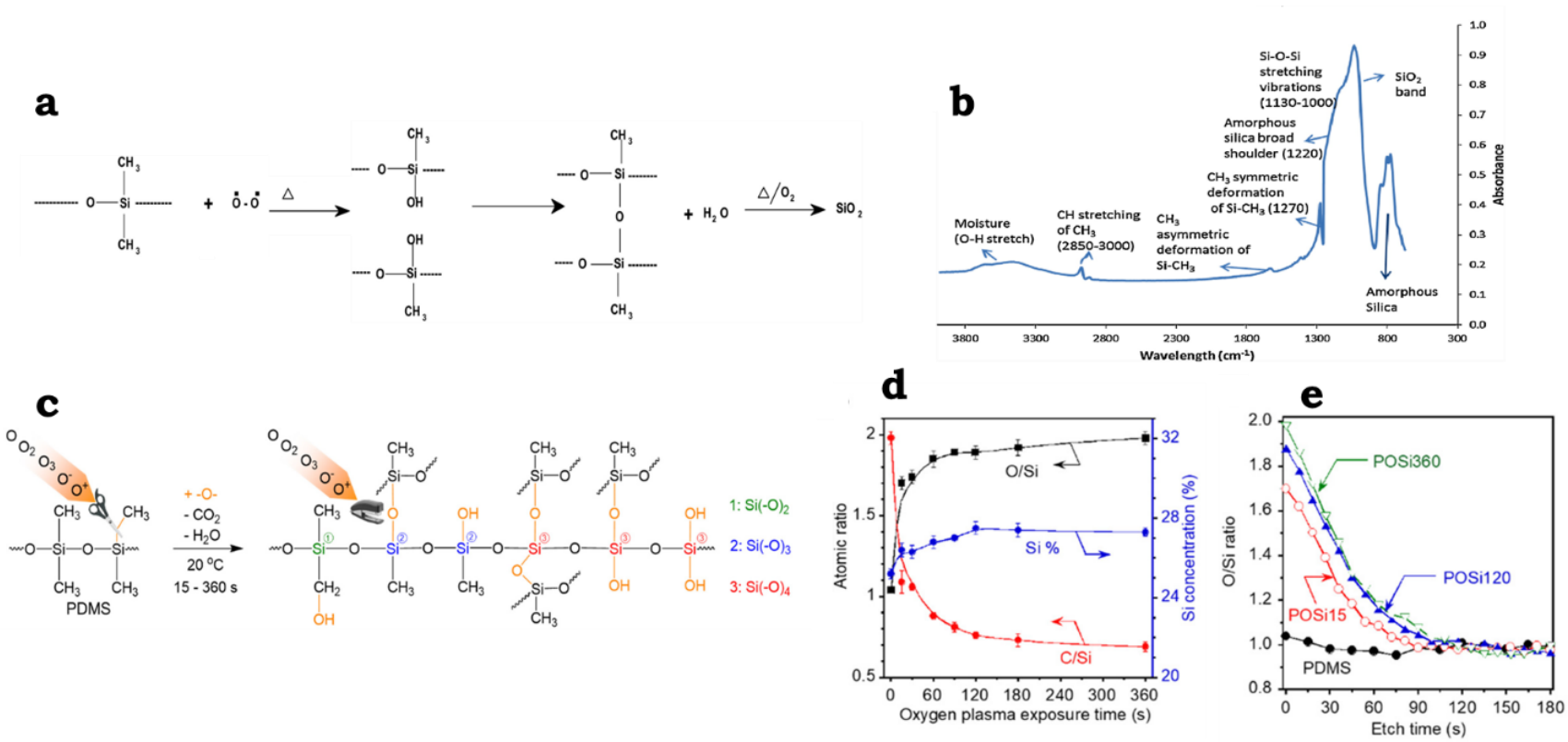

Fig. 7. (a) Thermal oxidation of PDMS/TEOS films. (b) FTIR spectrum of thermally oxidized PDMS/TEOS film. Copyright (2011) Elsevier [87]. (c) Schematic of conversion of PDMS into organosilica by the oxygen plasma. (d) Influence of oxygen plasma exposure time on the membrane surface chemistry. (e) Gradient change in the O/Si ratio along the membrane thickness. Copyright (2021) American Chemical Society [14].

3. Transport mechanisms in silica membranes

Molecular transport through silica membranes with sub-nm pore size is often described using the solution-diffusion (SD) model [76, 87-90] or the modified gas-translation (mGT) model [91-95]. The SD model assumes that the membranes are nonporous, and penetrants need to be dissolved in the membranes before diffusion. The model was successfully applied to describe gas transport in the silica membranes derived from the pyrolysis of PDMS/TEOS [87, 88] and amino-organosilica membranes [36, 90, 96]. By comparison, the mGT model assumes that the silica membranes have rigid and cylindrical pores for molecular diffusion [97, 98]. The following section will discuss the concept, derivation, and application of both models.

3.1. Solution-diffusion (SD) model

The SD model is widely used to describe gas permeation through nonporous materials. First, the penetrants dissolve into the membrane on the high chemical potential side (feed). Second, the molecules diffuse through the membrane because of the chemical potential gradient. Third, the molecules desorb on the low chemical potential side (permeate). Gas permeability (P) is the product of diffusivity (D) and solubility (S):

$$P = D \times S \tag{1}$$

The influence of the temperature (T) on gas permeability and diffusivity is described by the Arrhenius model:

$$P = P_0 \exp\left(-\frac{E_P}{RT}\right) \tag{2}$$

$$D = D_0 \exp\left(-\frac{E_{D,SD}}{RT}\right) \tag{3}$$

where R is the gas constant (J mol^{-1} K^{-1}), and P_0 and D_0 are the pre-exponential factors of permeability and diffusivity, respectively. E_P and $E_{D,SD}$ are the activation energy for permeation and diffusion, respectively. Gas solubility follows the Van't Hoff model:

$$S = S_0 \exp\left(-\frac{\Delta H_S}{RT}\right) \quad (4)$$

where S_0 is the pre-exponential factor of solubility, and ΔH_S is the apparent enthalpy of sorption. The ΔH_S can be expressed using equation 5:

$$E_p = E_{D,SD} + \Delta H_S \quad (5)$$

The $E_{D,SD}$ is usually positive, while ΔH_S is generally negative. Therefore, E_P can be either positive or negative, depending on the magnitude of $E_{D,SD}$ and ΔH_S.

Fig. 8a-d presents chemical structure and gas transport properties as a function of temperature for silica membranes prepared from thermal oxidation of PDMS/TEOS [88]. Increasing the temperature increased the permeability of H_2, He, O_2, N_2 and CH_4 but decreased CO_2 permeability as CO_2 exhibited a larger magnitude of ΔH_S (-20.4 kJ mol^{-1}) than E_D (16 kJ mol^{-1}) [88].

Fig. 8e-g presents another example of using the SD model to describe gas permeation in amino-organosilica membranes [90]. The strong interaction between CO_2 and amino functional groups was confirmed by the highly negative values of ΔH_S, i.e., -73.5, -68.5 and -63.1 kJ mol^{-1} for the membranes functionalized with primary amine (PA), secondary amine (SA), and ternary amine (TA), respectively. Fig. 8f displays the CO_2/N_2 selectivity versus CO_2 permeance in the membranes at different temperatures. Despite the lowest CO_2 affinity, the TA-functionalized membrane exhibited the most balanced CO_2 permeance of 600 GPU and CO_2/N_2 selectivity of 20 at 35 °C because of its fastest sorption-desorption cycle of 1.8 mins compared with 65.6 and 10.5 mins for PD- and SA-functionalized membranes, respectively (Fig. 8g).

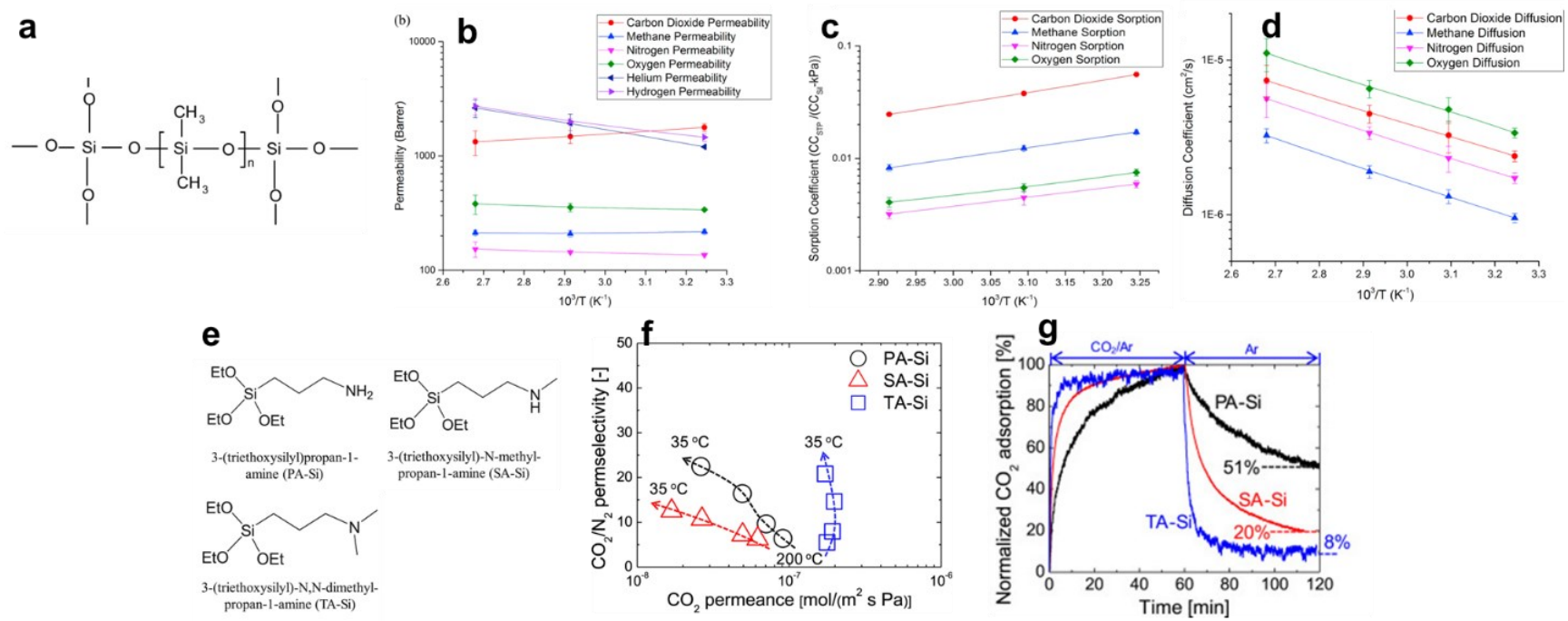

Fig. 8. (a) Chemical structure, (b) gas permeability, (c) gas sorption, and (d) gas diffusivity for PDMS/TEOS derived silica membranes. Copyright (2016) Elsevier [88]. (e) Chemical structures of amino decorated membrane precursors. (f) CO_2/N_2 selectivity as a function of CO_2 permeance at different temperatures and (g) normalized CO_2 adsorption over time of the amino-decorated membranes. Copyright (2017) Elsevier [90].

3.2. Gas translation (GT) model

The GT model assumes that molecules move between adsorption sites via translation mode in the pores with diameters larger than the penetrant size, overcoming the energy barriers existing in the channels between the adsorption sites. This translational movement exhibits a Knudsen-like diffusion and thus, the GT model is also considered as activated Knudsen diffusion. Permeance of gas *i* (Q_i) is expressed as [99]:

$$Q_i = \frac{\varepsilon d_p \rho}{\tau L}\left(\frac{8}{\pi M_i RT}\right)^{\frac{1}{2}} \exp\left(\frac{-E_{D,i}}{RT}\right) \tag{6}$$

where ε is the membrane porosity, d_p is the pore diameter (m), ρ is the probability of diffusion, τ is the tortuosity, L is the membrane thickness (m), and M_i is the penetrant molecular mass (kg mol^{-1}). For silica membranes, a modified GT (mGT) model is developed to consider the effective area for diffusion in the pores, and Equation 6 becomes [98, 100, 101]:

$$Q_i = \frac{k_{0,i}}{\sqrt{M_i RT}} \exp\left(-\frac{E_{D,i}}{RT}\right) \tag{7}$$

$$k_{0,i} = \sqrt{\frac{8}{\pi}}\,\frac{\varepsilon}{3\tau L}\,\frac{(d_p - d_i)^3}{d_p^2} \tag{8}$$

where $k_{0,i}$ is the geometric value, and d_i is the penetrant kinetic diameter (m).

The mGT model can be used to estimate the pore size of silica membranes. For example, Fig. 9a displays the schematic of the MTES membrane before and after water-plasma treatment, and Fig. 9b presents the temperature dependence of gas permeance, which was used to derive $k_{0,i}$ from Equation 7 [27]. Fig. 9c presents the fitting of $k_{0,i}$ using equation 8, yielding d_p values of 4.6 and 4.0 Å for the pristine MTES and plasma-treated MTES, respectively [27].

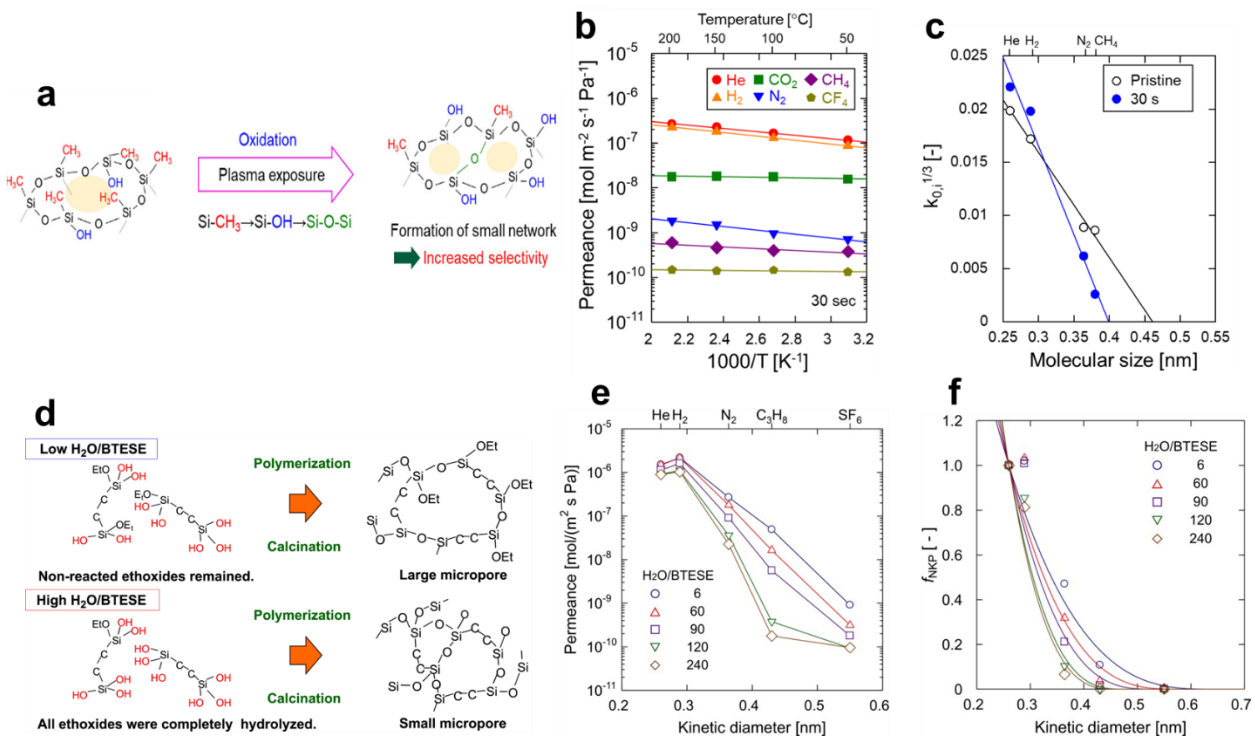

Fig. 9. (a) Schematic of the MTES membrane before and after water-plasma treatment. (b) Gas permeance at different testing temperatures. (c) Correlation between $k_{0,i}$ and d_i to derive d_p. Copyright (2022) American Chemical Society [27]. (d) Schematic for the effect of WR on the BTESE network structures. Copyright (2014) Elsevier [54]. (e) Gas permeance and (f) modeling using equation 9. Copyright (2014) American Institute of Chemical Engineers [97].

The mGT model can also be used to estimate d_p by Normalized Knudsen Permeation (NKP), as shown in Fig. 9d-f. In this method, f_{NKP} is calculated as the permeance ratio of a gas to a standard gas (such as He):

$$f_{NKP} = \frac{Q_i}{Q_{He}} = \frac{(d_p - d_i)^3}{(d_p - d_{He})^3} \exp\left(-\frac{E_{D,i} - E_{D,He}}{RT}\right) \tag{9}$$

Two assumptions are often made: (1) gas permeates through identical pores, and (2) the E_D values are similar for all gases. As such, Equation 9 is simplified to:

$$f_{NKP} = \frac{P_i}{P_{He}} \approx \frac{(d_p - d_i)^3}{(d_p - d_{He})^3} \tag{10}$$

Fig. 9e presents pure-gas permeance through the BTESE membranes prepared at different WR values [54, 97], and Fig. 9f displays the f_{NKP} values used to derive the d_p values. Increasing the WR value from 6 to 240 decreased the d_p from 6.5 to 4.6 Å [97].

Both SD and mGT models have been successfully used to interpret gas permeation data in silica membranes, though they describe different physical processes. The SD model relies on free volumes [87, 88], and the mGT model involves pore sizes [90, 93, 96, 102]. As neither parameter can be quantitatively determined, it is impossible to validate one model over the other.

3.3. Computational simulation for gas transport through silica membranes

Molecular dynamic simulation has been used to describe gas transport through pure silica and organosilica membranes. For instance, Stillinger–Weber three-body interactions and modified Born–Mayer–Huggins pair potential (SW-BMH) were used to construct pure silica structure, and nonequilibrium molecular dynamics (NEMD) was applied to simulate gas permeation [101, 103-105]. Fig. 10a presents the silica membranes with cylindrical pores [103]. Gas permeation through the pores with diameters of 6 - 9 Å followed Knudsen diffusivity except for CO_2 and C_3H_6, which showed permeance higher than predicted by Knudsen diffusivity because of their affinity toward the silica [101, 103]. For example, decreasing the pore diameter from 8 to 6 Å increased CO_2 interaction with the pore wall and thus CO_2/He selectivity from 0.85 to 1.64 at 77 °C [103]. Virtual silica membranes were also constructed to mimic TEOS-derived membranes with pore diameters between 6 and 11 Å to confirm the mGT model [101].

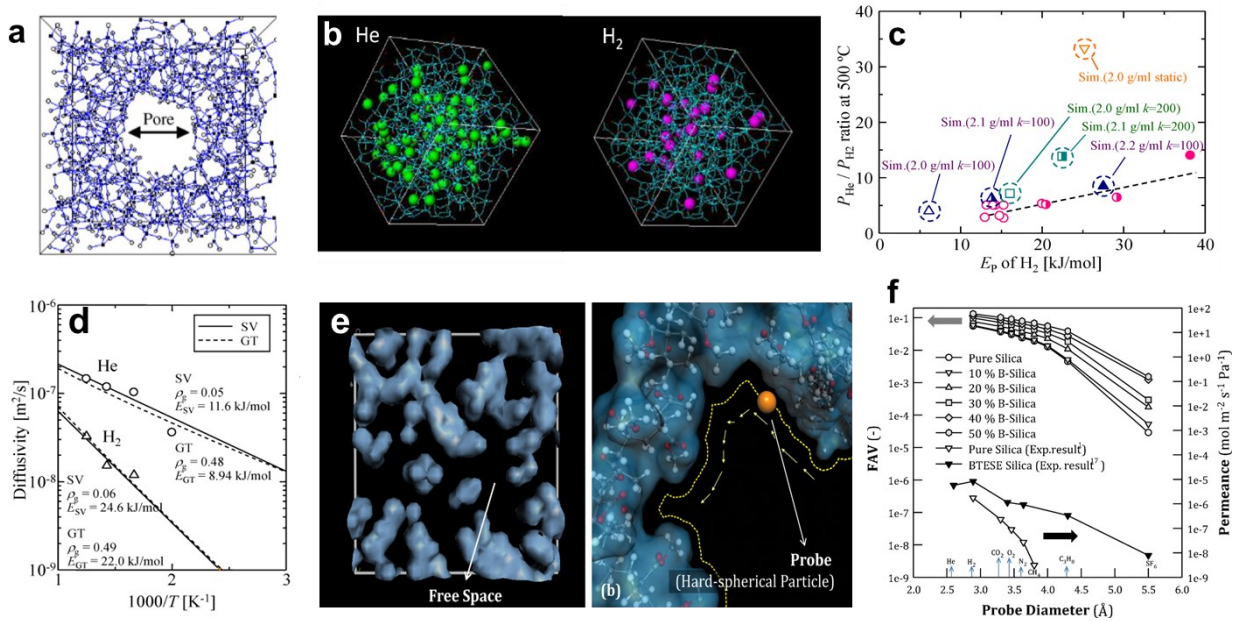

Fig. 10. (a) Snapshot of silica pore constructed using SW-BMH models. Copyright (2012) American Institute of Chemical Engineers [101]. (b) Snapshot of available sorption sites for He and H_2, generated by NEMD [105]. (c) He/H_2 selectivity as a function of activation energy of permeation for H_2 [105]. (d) Diffusivity of He and H_2 through virtual membrane fitted by the mGT and solid vibration model [105]. (e) Free space in TEOS/BTESE membrane constructed by the pcff-force field. (f) Effect of the BTESE content on fractional free volume and permeance. Copyright (2011) Elsevier [106].

Fig. 10b presents the structure of the silica network and accessible volume for He and H_2. He had a higher number of accessible volumes than H_2 because of its smaller kinetic diameter. Fig. 10c compares the He/H_2 selectivity as a function of H_2 E_P for simulated and experimental results. Increasing the silica density and thermal vibration increased He/H_2 selectivity and H_2 E_P. Silica with a density of 2.1 g/cm^3 and a thermal vibrational constant of 100 showed results similar to the experimental ones. Fig. 10d illustrates good fittings of the H_2 and He diffusivity using the mGT and solid vibration models [105].

For organosilica membranes such as TEOS/BTESE blends, hybrid polymer consistent force-field (h-pcff) molecular dynamics was used to construct the organic-inorganic structures, as shown in Fig. 10e [106, 107]. Increasing the BTESE content increased the mean-square

displacement and thus gas permeance because of the higher fractional accessible volume (FAV) and larger cavity size distribution (Fig. 10f) [106].

4. Silica precursors

Precursors are critical in forming silica structures. Fig. 11 presents the chemical structures of typical alkoxysilanes used to prepare pure silica and organo-alkoxysilanes used to synthesize organosilica membranes.

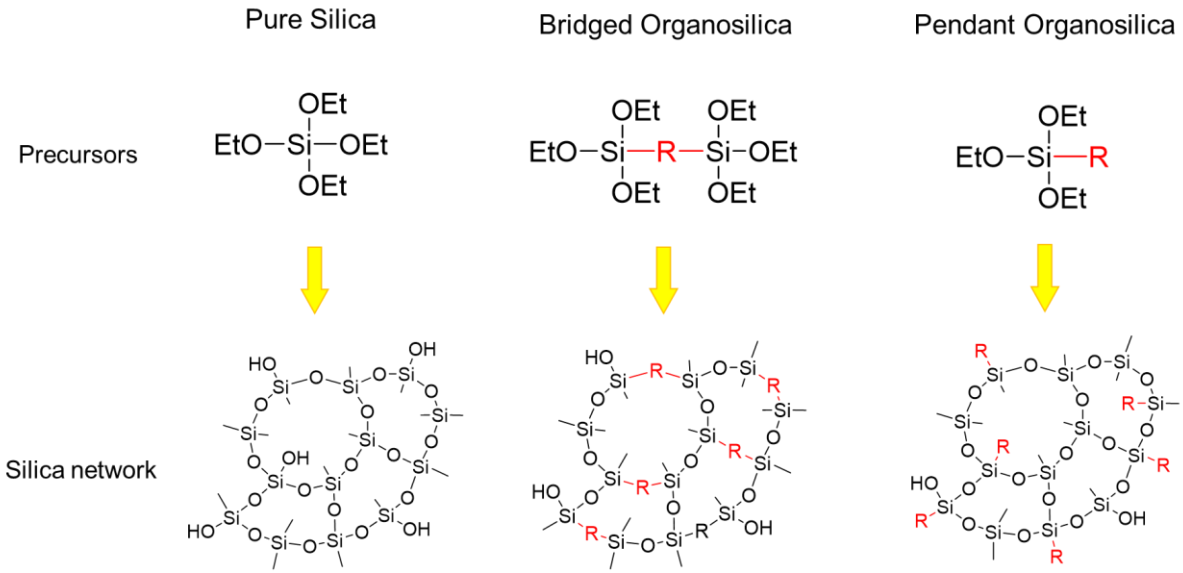

Fig. 11. Schematic comparing the pure silica, bridged organosilica, and pendant organosilica synthesized from alkoxysilanes, bridged organo-alkoxysilanes, and pendant organo-alkoxysilanes, respectively.

4.1. Pure silica membranes

Pure silica membranes can be synthesized from TEOS or tetramethyl orthosilicate (TMOS) via the sol-gel or CVD processes [38, 51, 76, 108-112]. These membranes exhibit tight networks with the strong molecular sieving ability [33, 38, 76, 79]. However, pure silica is known for its poor stability in hydrothermal conditions due to the hydrolysis of siloxane linkages (e.g., the reverse direction of Reaction 3) [51, 94, 113]. Fig. 12 illustrates that water hydrolyzed

siloxane linkages to form mobile silanol groups, which were then condensed to form tight structures, decreasing gas permeance without improving size-sieving ability [114]. For example, after TEOS-derived silica membranes were exposed to 16 mol% water at 600 °C for 72 h, H_2 permeance decreased by 68% from 450 to 140 GPU and H_2/N_2 selectivity decreased from 1500 to 1000 [115]. Similar behavior was also observed in other studies of TEOS-derived silica membranes [116, 117].

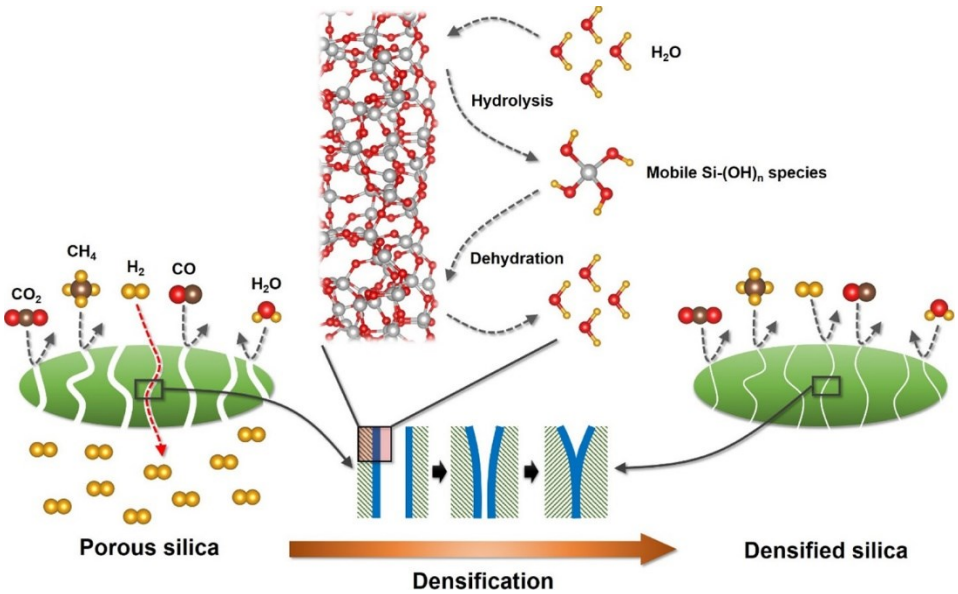

Fig. 12. Schematics for the densification of silica membranes under hydrothermal conditions. Copyright (2019) American Chemical Society [114].

4.2. Organosilica membranes

Silica membranes can be incorporated with hydrophobic organic groups (i.e., organosilica) to improve hydrothermal stability. For example, BTESE with hydrophobic ethyl linkages (e.g., Si-CH_2CH_2-Si) was investigated for reverse osmosis [118-121], pervaporation dehydration [122, 123] and vapor permeation [68, 124], due to its excellent hydrothermal stability. Fig. 11 shows schematic structures of bridged and pendant organosilica. The chemical structures of the precursors and the resultant membrane pore dimensions are also summarized in Table 1.

The pore size of the bridged organosilica can be easily tuned by controlling the organo-bridging units. For example, increasing the carbon number from 1 in BTESM to 8 in BTESO increased the NKP pore size from 4.7 to 7.1 Å and thus gas permeance and decreased H_2/N_2 selectivity [93]. On the other hand, functional groups (such as vinyl [115], amine [90, 125], and fluorine [40, 126]) can be incorporated in pendant organo-alkoxysilanes to manipulate hydrophilicity and affinity towards specific penetrants. For instance, organosilica membranes with pedant fluorine group prepared from triethoxyfluorosilane (TEFS) exhibited lower Si-OH content and thus greater hydrophobicity than those prepared from TEOS [40, 126].

Table 1.
Chemical structures of silica precursors and the pore structures of the resultant membranes.

Precursors	Structure	Fabrication	Surface area (m^2 g^{-1})	Pore diameter (Å)	Pore volume (cm^3 g^{-1})
Pure silica					
TEOS [76]		sol-gel	-	3.6 – 5.5	0.28
TRIES [59]	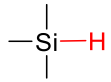	sol-gel	-	5.77	-
Bridged organosilica					
BTESM [127, 128]	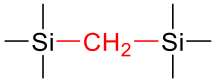	sol-gel	597	3.6 - 5.3	0.342
BTESE [94]	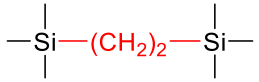	sol-gel	222 - 338	3.62 – 4.54	0.114 – 0.173
BTESEthy [92]	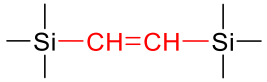	sol-gel	556	4.3	0.31
BTESA [92]	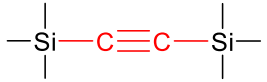	sol-gel	594	5.2	0.33
BTESB [91]	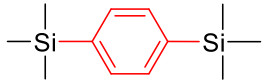	sol-gel		4.6	
BTESBPh [91]	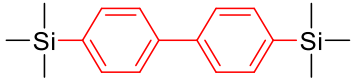	sol-gel		6	
BTES-ED [129]	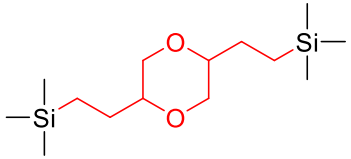	sol-gel	373	8 – 16	-
BTMSN [130]	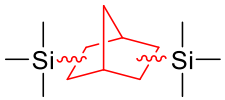	sol-gel	336	~ 6	-

BTPP [96]	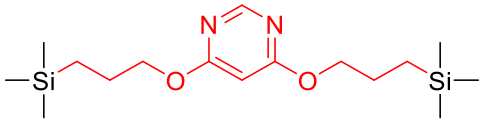	sol-gel	0.2145	5.7	0.049
BTES-MOU [131]	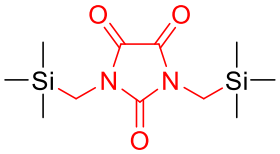	sol-gel	155	-	-
BTES-POU [131]	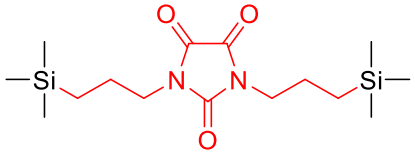	sol-gel	10	-	-
BTESPA [70]	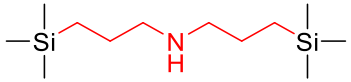	sol-gel	176	-	0.18
Pendant organosilica					
APTES [90]	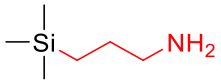	sol-gel	< 1	-	~ 0
HMDSO [86]	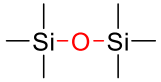	PE-CVD	-	4 – 6	-
MTES [75]	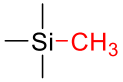	sol-gel	-	5.2	-
PhTES [91]	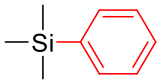	sol-gel	-	4.5	-
SA-Si [90]	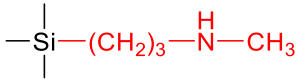	sol-gel	< 1	-	~ 0
TA-Si [90]	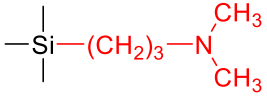	sol-gel	< 1	-	~ 0
TEFS [40]		sol-gel	215 – 275	-	-

TPMS [132]	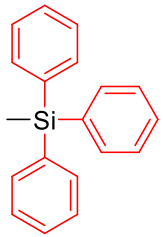	PE-CVD	-	4.86	-
DPhDMOS [132]	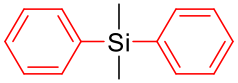	PE-CVD	-	4.2	-
VTES [115]	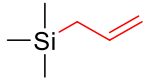	CVD	-	~ 3.8	-

5. Silica membranes for gas separations

Silica membranes have been widely explored for various gas separations due to their tunable and robust porous structure, allowing precise molecular separation. The following sections highlight the recent advancement of silica membranes for various separations, such as H_2/CO_2, CO_2/N_2, and C_3H_6/C_3H_8.

5.1. H_2/CO_2 separation

Silica membranes exhibit very attractive H_2/CO_2 separation properties due to their unique pore structures compared to polymeric or other inorganic membranes, as shown in Table 2.

Table 2
Representative silica membranes with attractive H_2/CO_2 separation properties.

Membrane materials	Fabrication	Temp. (°C)	H_2 permeance (GPU)	CO_2 permeance (GPU)	H_2/CO_2 Selectivity
Pristine					
BTESE [94]	sol-gel	200	48	1.3	36.4
DMDMS [80]	CVD	500	960	0.75	1280
MTMOS [81]	CVD	600	720	0.24	3000
TMOS [80]	CVD	500	290	0.13	~ 2200
VTES [115]	CVD	600	1600	17	95
Metal doping					
Co-TEOS [89]	sol-gel	250	18	0.018	~1000
Nb -TEOS [133]	sol-gel	200	1900	41	46
Pd - TEOS [134]	sol-gel	200	1200	75	16
Ti - BTESM [135]	sol-gel	200	510	21	24
Nb - BTESE [136]	sol-gel	200	280	1.3	220
Pd - BTESE [137]	sol-gel	200	3000	170	17.2
Zr - BTESE [138]	sol-gel	200	540	34	16
Pd-Nb - BTESE [62]	sol-gel	200	~ 1200	75	16
Plasma Treatment					
PDMS [14]	Oxygen-plasma	150	280	3.0	93

CVD is an effective way to generate tight structures because of the small building blocks. For example, silica membranes prepared from vinyltriethoxysilane (VTES) with a pendant vinyl

group exhibited H_2 permeance of 1620 GPU and H_2/CO_2 selectivity of 95 at 600 °C [115]. Additionally, membranes prepared from the precursors with methyl pendant groups (such as tetramethyl orthosilicate (TMOS), methyltrimethoxysilane (MTMOS), and DMDMOS) showed H_2/CO_2 selectivity of more than 1000 (Table 1) [80, 81].

Higher calcination temperature increases the condensation degree and induces denser silica networks with stronger molecular sieving ability [77, 78, 94]. For instance, increasing the calcination temperature from 550 to 700 °C for TEOS-derived membranes decreased the pore size from 3.85 to 3.47 Å [78]; increasing the calcination temperature from 400 to 600 °C increased H_2/CO_2 selectivity from 27 to 70 at 200 °C [38]. For BTESE-derived organosilica membranes, increasing the calcination temperature from 400 to 600 °C decreased the pore diameter from 4.54 to 3.62 Å and increased H_2/CO_2 selectivity from 9.5 to 36 [94].

Incorporating metals into silica membranes can improve separation performance, and it is often achieved by introducing metal alkoxide or metal salts into the sol solution. The metals in silica have two forms: metal ions or embedded metal/metal oxide particles [62, 117, 134, 139, 140]. Metal ions can form covalent linkages with silica networks, decreasing pore sizes. For example, doping TEOS membranes with Mg^{2+} decreased the pore size from ~ 5 to < 3 Å and decreased H_2 permeance from 1600 to 210 GPU but drastically enhanced the H_2/CO_2 selectivity from 9 to >350 [141]. Similarly, doping the BTESE membrane with Nb^{+} reduced the surface area from 120 to 26.8 m^2 g^{-1} and improved H_2/CO_2 selectivity from ~3 to 220 [136, 140]. Additionally, the covalent linkages can stabilize the silica networks and enhance the resistance to hydrothermal degradation. For instance, the Co-doped TEOS membrane showed stable H_2/N_2 selectivity of 300 for a 60-h test at 500 °C and water vapor of 300 kPa [117].

Palladium (Pd) was incorporated into TEOS [134, 142] and BTESE [137, 143] membranes because of its affinity toward H_2. However, the Pd doping in BTESE decreased H_2/CO_2 selectivity from 7.3 to 4.3 at 200 °C because of the voids between the Pd nanoparticles and silica networks [137]. Similarly, PdO was reduced after exposure to H_2 and aggregated in TEOS membranes, which increased H_2 permeance and decreased H_2/CO_2 selectivity [134]. Interestingly, Figure 13 shows that the bi-metallic doping of Pd-Nb of BTESE increased both H_2 permeance and H_2/CO_2 selectivity because the Pd exist as nanoparticles with affinity towards H_2, and Nb formed Nb-O-Si covalent bonds to tighten the networks [62]. Fig. 13b presents H_2/CO_2 separation performance of Pd-Nb doped BTESE using different synthesis pathways.

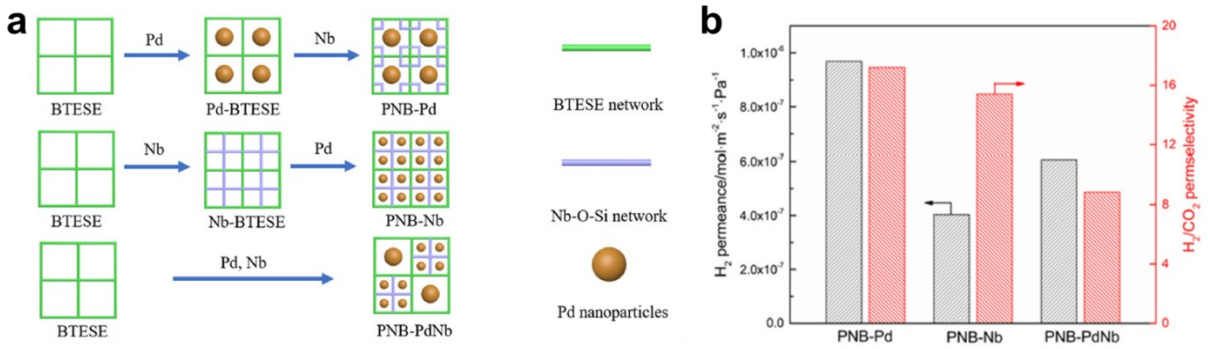

Fig. 13. Pb-Nb doped BTESE networks. (a) Schematic showing that Pd exists as particles and Nb formed Nb-O-Si. (b) H_2 permeance and H_2/CO_2 separation properties. Copyright (2020) Chemical Industry Press Co. [62].

Oxygen plasma-treated PDMS was demonstrated to form silica membranes with superior H_2/CO_2 separation properties [14]. Specifically, PDMS was coated on polybenzimidazole (PBI) porous supports followed by rapid (< 360 s) oxygen-plasma treatment at low pressures to form polyorganosilica membranes (POSi). Fig. 14a presents the cross-sectional SEM image. Increasing the plasma exposure time from 15 to 360 s increased H_2/CO_2 selectivity from 10 to 93 at 150°C (Fig. 14b). Additionally, the oxygen plasma treatment retained a high content of methyl groups in POSi networks with the CH_3/Si molar ratio of 0.61, attributing to the strong

hydrothermal stability. The membrane showed stable performance in the presence of 0.6 mol% water at 200 °C (Fig. 14c) and excellent resistance to aging up to 350 days (Fig. 14d).

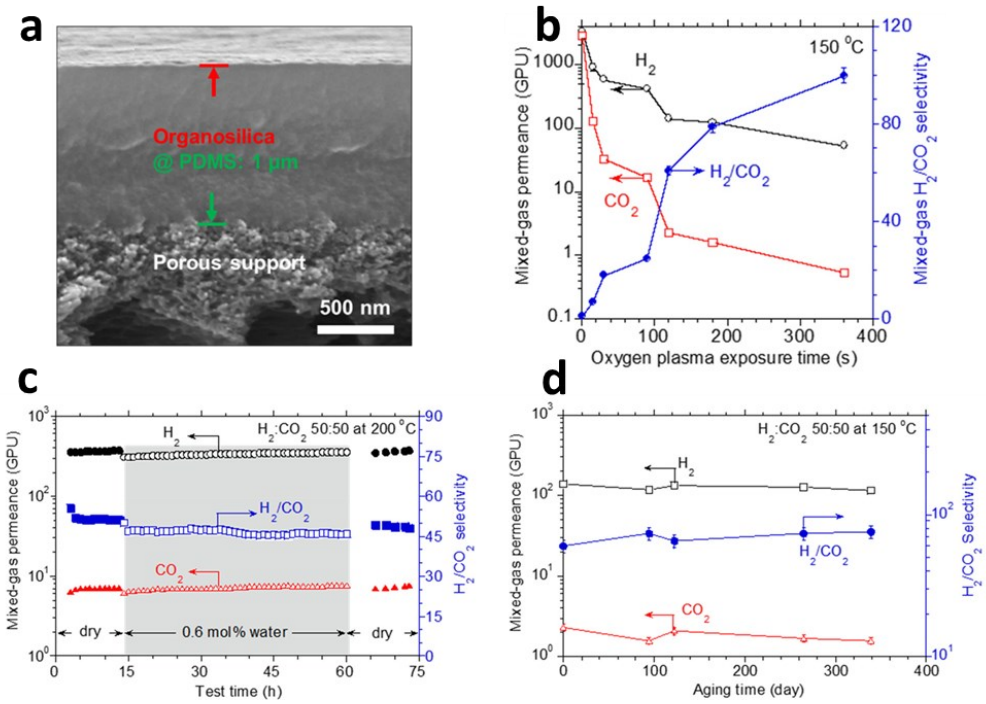

Fig. 14. (a) Cross-sectional SEM image of POSi membrane. (b) Mix-gas H_2/CO_2 separation performance as a function of the plasma exposure time. (c) Stable separation performance in wet conditions. (d) Long-term stability. Copyright (2021) American Chemical Society [14].

5.2. CO_2/N_2 separation

Table 3 highlights the recent development of organosilica membranes for CO_2/N_2 separation.

Table 3
Representative organosilica membranes with attractive CO_2/N_2 separation properties.

Membrane materials	Fabrication method	Temp. (°C)	CO_2 permeance (GPU)	N_2 permeance (GPU)	CO_2/N_2 selectivity
Pristine					
BTESA [144]	sol-gel	100	3450	160	22
BTESB [91]	sol-gel	50	2600	77	34
PhTES [91]	sol-gel	50	1100	36	30
HMDSO [83]	PE-CVD	50	570	12	46
Precursors blending					
APTES - BTESA [145]	sol-gel	50	2600	61	42
BTPP – BTESE [96]	sol-gel	35	2100	110	20
BTESE – MTES [146]	sol-gel	30	600	21	29
BTESA – BTESB [147]	sol-gel	50	5500	220	25
Fluorine doping					
F - TEOS [148]	sol-gel	50	480	9.6	50

Bridged organoalkoxysilanes have a greater distance between Si atoms than pendant organosilica, inducing looser networks and thus a higher gas permeance. However, organosilica with long and flexible linear organic groups with carbon numbers greater than 3 showed non-porous behavior, lowering gas permeance [12, 93, 149]. On the other hand, bulky and rigid phenyl bridging units, such as bis(triethoxysilyl)benzene (BTESB) and 4,4′ -bis(triethoxysilyl)-1,1′-biphenyl (BTESBPh), can form robust pore structures for CO_2/N_2 separation. For instance, increasing the phenyl bridging units from 1 in BTESB to 2 in BTESBPh increased the pore diameter from 4.6 to 6.0 Å and CO_2 permeance from 2600 to 5580 GPU but decreased CO_2/N_2 selectivity from 34 to 13 [91]. Interestingly, blending BTESB with 1,2-bis(triethoxysiyl)acetylene (BTESA) with acetylene bridging units at 1:1 molar ratio decreased CO_2 permeance from 6000 to 2400 GPU but increased CO_2/N_2 from 13 to 25. On the other hand, blending BTESA with BTESBPh (BTESA-BPh, Fig. 15a,b) led to ultrahigh CO_2 permeance of 9700 GPU with a moderate CO_2/N_2 selectivity of 12, which was ascribed to the steric hindrance of the two aromatic rings in BTESBPh and thus large voids generated [147].

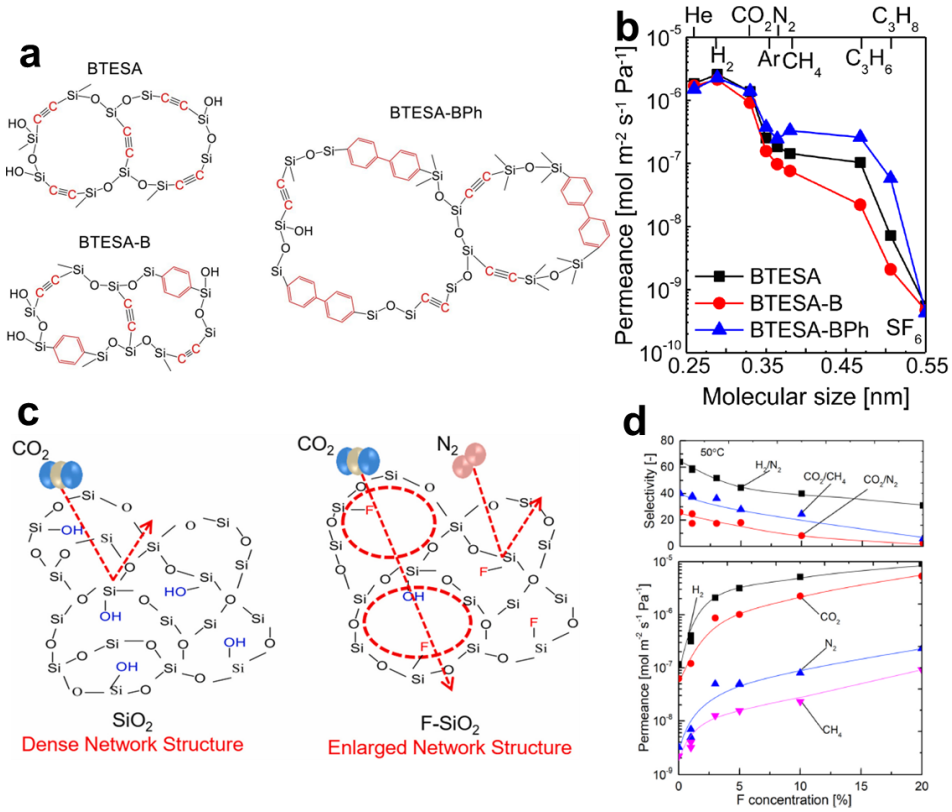

Fig. 15. (a) Schematic of BTESA, BTESA/BTESB, and BTESA/BTESBPh structures and (b) their pure-gas transport properties at 200 °C. Copyright (2021) Elsevier [147]. (c) Schematic for TEOS structural tuning via fluorine doping and (d) pure-gas transport properties of F-doped TEOS membranes at different F-loadings and 50 °C. Copyright (2022) Elsevier [148].

Fluorine doping of TEOS membranes also led to attractive CO_2/N_2 separation performance. For instance, doping TEOS membrane with 1 mol% of fluorine increased the CO_2 permeance from 186 to 480 GPU and CO_2/N_2 selectivity from 26 to 50 at 50 °C (Fig. 15c,d) [148]. The technique was achieved by the addition of NH_4F into the sol solution during the sol-gel synthesis. The -F groups replaced -OH groups to form Si-F bonding, reducing condensation degree and loosening the silica networks [12, 148, 150]. Additionally, the lower silanol content reduced densification at higher temperatures in the presence of water vapor [12, 148, 150].

CO_2-philic amino-alkoxysilanes can be incorporated to enhance CO_2 permeance [36, 90, 125, 145, 151]. However, these amine groups are long and flexible, which might block pores and

lower gas permeance [90, 145, 151]. To mitigate the blocking, the silica structure with enhanced rigidity and porosity can be achieved by precursor blending, which also enhanced amine accessibility to CO_2. Fig. 16a presents the schematic of BTPP, BTPP/TEOS, and BTPP/BTESE network structures. The incorporation of rigid TEOS and BTESE disrupted the π-π stacking of aromatic rings in BTPP, inducing microporosity to improve gas permeance (Fig. 16b) [96]. For instance, the incorporation of TEOS and BTESE in BTPP increased CO_2 permeance by roughly 20 folds and decreased CO_2/N_2 selectivity from 26 to 19 at 35 °C. Similar behaviors were observed for the APTES/BTSEA blends. APTES had long and flexible aminopropyl groups, leading to nonporous structure. The incorporation of BTESA with rigid acetylene groups generated porous structures, leading to CO_2 permeance of 2400 GPU, CO_2/N_2 selectivity of 25, and CO_2/CH_4 selectivity of 70 [145].

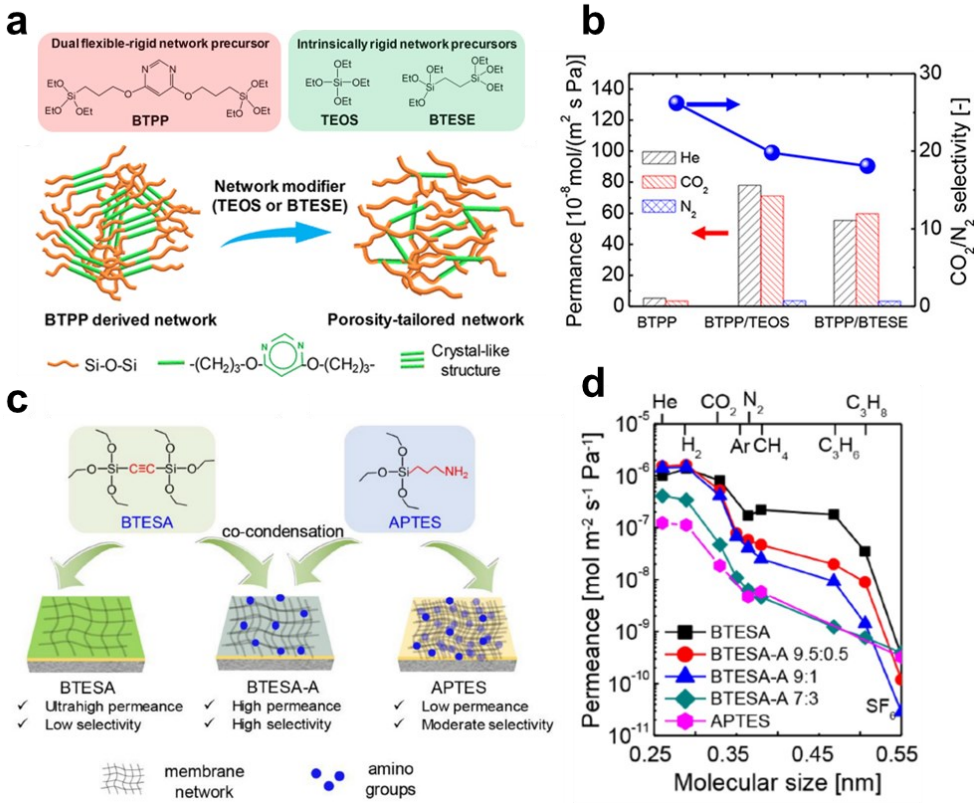

Fig. 16. (a) Schematic of BTPP-TEOS and BTPP-BTESE structure and (b) CO_2/N_2 separation performance at 35 °C. Copyright (2019) American Chemical Society [96]. (c) Porosity control of

amino-organosilica via the addition of rigid BTESA structure and (d) their pure gas permeance at 50 °C. Copyright (2020) Elsevier [145].

5.3. Separation of He and H_2 from other gases

Helium extraction from natural gas and H_2 recovery from dilute streams are important applications and involve their separation from larger gases like N_2, hydrocarbons, and organic vapors. With unique porous structures silica membranes can achieve high gas permeance and strong molecular sieving ability, as shown in Table 4.

Table 4
He and H_2 separation properties over N_2 and CH_4 in representative silica membranes.

Membrane materials	Fabrication	Temp. (°C)	He permeance (GPU)	He/N_2 selectivity	He/CH_4 selectivity	H_2 permeance (GPU)	H_2/N_2 selectivity	H_2/CH_4 selectivity
Pristine								
TEOS [38]	sol-gel	200	--	--	--	1490	> 135	> 4000
BTESM [93]	sol-gel	200	3300	~55	120	4200	70	150
BTESE [77]	sol-gel	300	--	--	--	1620	350	920
BTESEthy [92]	sol-gel	200	3600	36	120	4500	45	150
BTESB [65]	sol-gel	200	2400	80	84	--	--	--
DMDMS [80]	CVD	500	2400	> 5000	> 5000	840	2300	> 2000
HMDSO [83]	PE-CVD	50	330	196	--	--	--	--
TRIES [59]	sol-gel	300	600	1000	2000	--	--	--
VTES [115]	CVD	600	--	--	--	1620	170	480
Precursors blends								
MTES/BTESE [146]	sol-gel	30	--	--	--	1500	64	74
TMMOS/TEOS [152]	CVD	300	--	--	--	2490	100	140
Metal doping								
Co-TEOS [117]	sol-gel	500	1300	1800		533	730	--
Nb- TEOS [133]	sol-gel	200	1890	150	550	1830	150	550
Ni-TEOS [153]	sol-gel	500	2130	1450	--	610	400	--
Pd- TEOS [134]	sol-gel	500	580	100	--	1500	260	--
Zr-BTESE [139]	sol-gel	200	--	--	--	2400	55	80
Fluorine doping								
F-TEOS [148]	sol-gel	50	--	--	--	9000	45	> 100
Incorporating fillers								
BTESE/r-GO [154]	sol-gel	150	--	--	--	750	> 100	> 200
BTESE/ZIF-7 [155]	sol-gel	200	--	--	--	2400	159	> 200
BTESE/ZIF-8 [156]	sol-gel	25	--	--	--	3000	30	35
BTESE/MIL-53-NH_2 [156]	sol-gel	25	--	--	--	600	25	30

Since He and H_2 are much smaller than N_2 and CH_4, pure silica and organosilica membranes can achieve high selectivity. For example, pure silica membranes derived from TEOS exhibited H_2 permeance of 1490 GPU with H_2/N_2 selectivity of > 135 and H_2/CH_4 selectivity of > 4,000 at 200 °C [38]. By contrast, BTESM [93] and BTESEthy [92] had looser structures than TEOS and thus higher H_2 permeance (4200 and 4500 GPU, respectively) and lower H_2/CH_4 selectivity (150). Additionally, the molecular sieving ability of organosilica membranes can be improved by calcination at higher temperatures. For example, increasing the calcination temperature from 300 to 700 °C for BTESE membranes decreased H_2 permeance from 3000 to 1600 GPU and increased H_2/N_2 selectivity from 100 to 350 and H_2/CH_4 selectivity from 100 to 920 [77].

Precursor blending can be used to improve separation performance. For example, BTESE networks were tightened by copolymerization with smaller alkoxysilane building blocks, such as MTES [146], TEOS [157], and BTESM [158]. For instance, the addition of MTES in BTESE networks improved H_2 permeance from 600 to 1500 GPU and H_2/CH_4 selectivity from 45 to 75 [146]. On the other hand, adding TMMOS into TEOS-derived pure silica networks increased hydrothermal stability [152]. Specifically, a 100-hour hydrothermal exposure decreased H_2 permeance by 90% and H_2/N_2 selectivity by 80% for pristine TEOS membrane; by contrast, it decreased H_2 permeance by only 42% and H_2/N_2 selectivity by only 48% for TMMOS/TEOS membrane. The improved hydrothermal stability was attributed to the enhanced hydrophobicity induced by the methyl groups of TMMOS [152].

Nanofillers have been incorporated into silica membranes to form mixed matrix membranes (MMMs) to improve He/gas and H_2/gas separation performance, such as 2D graphene oxides (GOs) [154] and 3D materials (including MOFs [155, 156] and polyhedral

oligomeric silsesquioxane (POSS) [159-161]). Fig. 17a displays that the MMMs containing reduced GO (rGO) nanosheets in BTESE networks exhibited H_2 permeance of 17,000 GPU and H_2/N_2 and H_2/CH_4 selectivity of 120 and 223, respectively [154]. The strong molecular sieving was attributed to the increased tortuosity from the impermeable rGO and the high degree of silanol condensation of the silica networks stimulated by the rGO confinement [154].

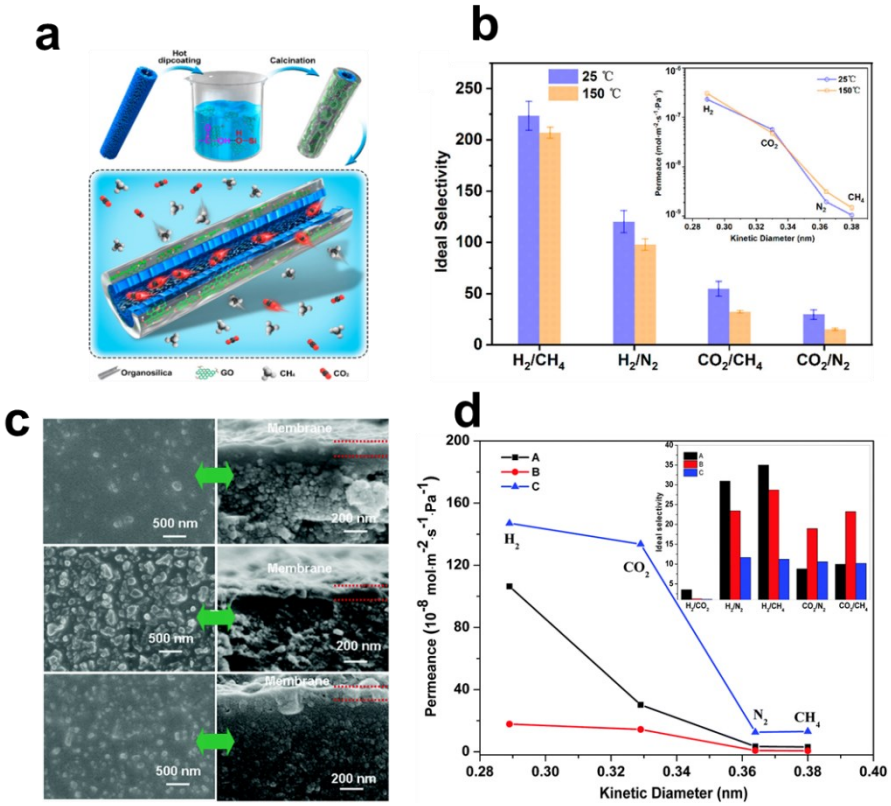

Fig. 17. (a) Schematic and (b) pure-gas separation performance of the MMMs containing rGO in BTESE [154]. (c) Surface and cross-sectional SEM images and (d) gas transport properties of the MMMs containing MOFs in BTESE. Copyright (2017) Royal Society of Chemistry [156].

Fig. 17c presents the SEM images of ZIF-8, MIL-53-NH_2, and CAU-1-NH_2 incorporated in BTESE [156]. The CAU-1-NH_2/organosilica exhibited the highest H_2 permeance of 4410 GPU due to the largest pore diameter (3 - 4 Å) and highest porosity. However, the MMMs containing ZIF-8 exhibited the highest H_2/CH_4 selectivity of 35, compared with those containing MIL-53-NH_2 (28) or CAU-1-NH_2 (12). The MMMs containing MIL-53-NH_2 exhibited a

balanced CO_2 permeance of 450 GPU and CO_2/CH_4 selectivity of 23 [156]. Similarly, the incorporation of ZIF-7 nanoparticles in BTESE increased H_2/CO_2 selectivity from 5.7 to 23 while retaining H_2 permeance at 2400 GPU [155].

5.5 C_3H_6/C_3H_8 separation

Fig. 18a presents organosilica precursors with different saturation degrees for C_3H_6/C_3H_8 separation, BTESE (C–C), BTESEthy (C=C), and BTESA (C≡C) [92]. Increasing the saturation degree decreased O-Si-O bond angles and the pore size, as indicated by 5.2 Å for BTESA, 4.3 Å for BTESEthy, and 4.2 Å for BTESE. Fig. 18b compares these organosilica membranes with other inorganic materials for C_3H_6/C_3H_8 separation performance [92]. The BTESA exhibited the most balanced performance with C_3H_6 permeance of 300 GPU and C_3H_6/C_3H_8 selectivity of 12 at 50 °C [92], and blending by BTESB with benzene rings tightened the pore structures, decreased C_3H_6 permeance to 135 GPU, and increased C_3H_6/C_3H_8 selectivity to 33 [65].

Silica membranes can be functionalized to enhance C_3H_6 affinity to improve C_3H_6/C_3H_8 separation properties. For example, Fig. 18c presents that hydrothermal treatment of TEFS membranes improved C_3H_6 adsorption capacity but had no impact on C_3H_8 adsorption because the steam treatment increased the adsorption sites (i.e., Si-OH) for C_3H_6. Fig. 18d displays the TEFS silica membranes with only a slight decrease in pure-gas permeance after hydrothermal treatment, which was attributed to the fluorine groups that reduced silanol condensation and avoided pore collapse [40]. Consequently, hydrothermal treatment enhanced C_3H_6/C_3H_8 selectivity from 20 to 42 at 35 °C. Similarly, low calcination temperatures (such as 150 °C) for BTESA membranes retained high Si-OH content, leading to C_3H_6 permeance of 51 GPU and C_3H_6/C_3H_8 selectivity of 52 at 50 °C [162].

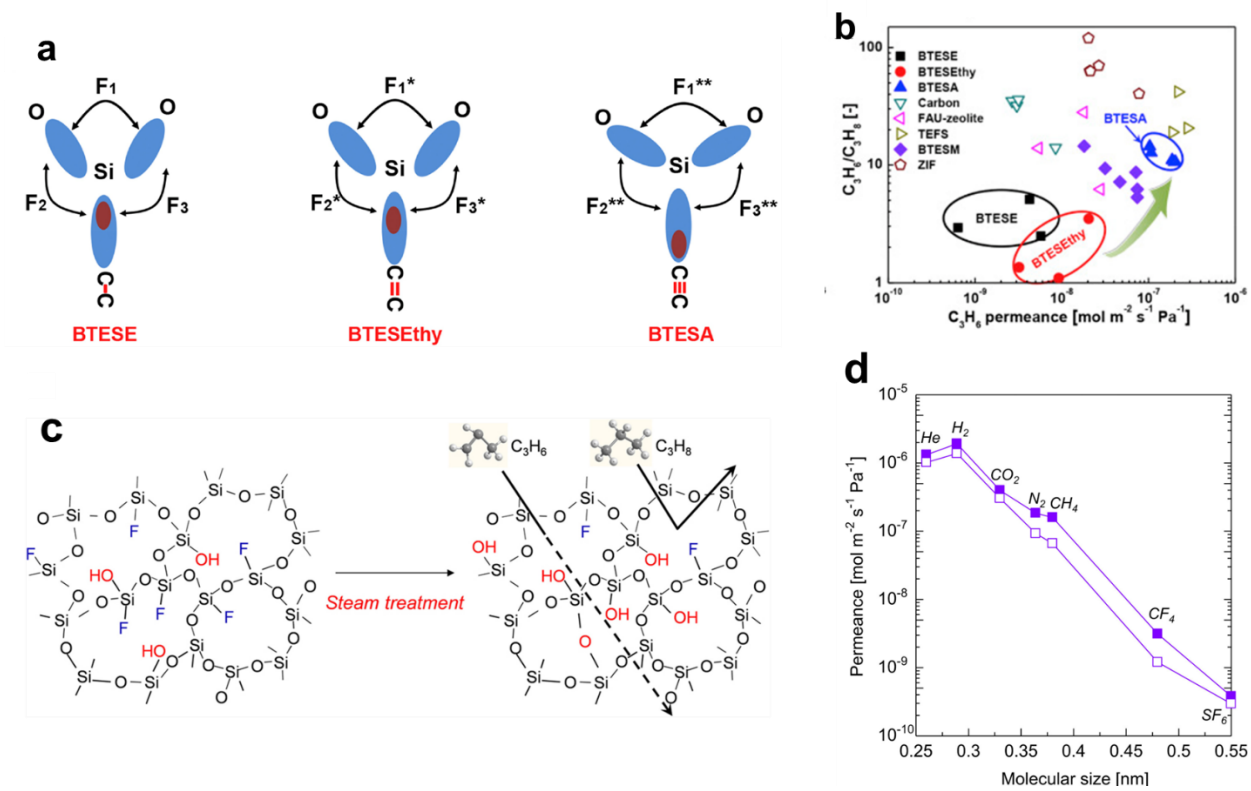

Fig. 18. (a) Influence of carbon bridge saturation degree on the O-Si-O linkage angles. (b) C_3H_6/C_3H_8 separation performance of BTESE, BTESEthy, and BTESA. Copyright (2019) Elsevier [92]. (c) Schematic of TEFS structure after the steam treatment at 30 kPa and 300 °C. (d) Pure-gas permeance before (close symbols) and after (open symbols) steam treatment of TEFS membrane at 300 °C. Copyright (2017) Elsevier [40].

6. Silica membranes for liquid separations

With robust porous structures and high chemical resistance, organosilica membranes have been investigated for liquid separations, such as solvent dehydration and desalination of salty water. Compared to silica membranes for gas separations, organosilica membranes for liquid separation have large pores and excellent stability in liquids (such as water or organic liquids). First, the large building block of organo-alkoxysilanes and the wide selection of organic groups result in membranes with large and tunable porous structures suitable for liquid separation. Second, the hydrophobic organic groups in organosilica protect siloxane backbones against hydrolysis by shielding them from water, and thus enhancing their resistance to

hydrothermal degradation [77, 122]. We have highlighted several approaches developed to improve separation performance and hydrothermal stability, such as functionalization with hydrophobic groups, metal doping, and carbon template.

6.1. Solvent dehydration by pervaporation

Pervaporation membranes have been widely explored for organic solvent dehydration, as only a small portion of the feed solution (mainly water) needs to be vaporized on the permeate side, leading to high energy efficiency compared with distillation (which needs vaporization of the whole feed solution) [163, 164]. Polymeric membranes are often used due to their high processibility, but they can be swollen by the solvents and lose their size-sieving ability. By contrast, silica membranes with rigid inorganic structures exhibited excellent resistance to swelling and retained strong molecular sieving ability. Therefore, several silica-based membranes have been commercialized for solvent dehydration, such as ECN [22, 165], HybSi® [166-168], Pervatech [26, 165, 169], and Pervap SMS [24, 25, 170], as summarized in Table 5. These membranes have thin selective layers (less than 500 nm) of organosilica with excellent hydrothermal stability. For example, HybSi® membranes derived from the blends of BTESE, BTESM and MTES demonstrated stable butanol dehydration performance at 150 °C for up to 1000 days of continuous operation [166]. These membranes have been investigated for dehydration of more than 30 organic solvents, such as alcohols, acids, and ketones [22, 165, 171, 172], and they showed separation performance competitive with zeolitic membranes [24, 26, 172].

Table 5
Pervaporation performance of solvent dehydration in representative organosilica membranes.

Membrane Material	Operating conditions		H_2O in feed (%)	H_2O flux (kg m^{-2} h^{-1})	H_2O permeance (GPU)	Solvent permeance (GPU)	Separation performance	
	Solvent	Temp. (°C)					H_2O/solvent selectivity	H_2O/solvent separation factor
Commercial membranes								
ECN [22]	Ethanol	70	3.5	1.5	1000	26	38	350
	IPA	80	4.5	1.9	1000	-	-	1150
	n-Butanol	75	5.0	4.5	91,000	-	-	600
	Acetone	50	10	0.8	580	-	-	33
	DMF	75	5	0.2	690	-	-	24
	THF	60	5	5.8	3700	-	-	150
HybSi® [23]	n-Butanol	95	5	2.0-3.6	1800-3300	-	-	4700
Pervatech [26]	IPA	75	9.8	2.6	1800	1.3	1400	190
Pervap SMS [24, 25]	Acetone	40-70	0-30	< 1.4	< 760	-	-	0.5-1.1
	t-Butanol	100	5.6	1.2	310	-	-	560
Emerging membranes								
BTESE [58]	n-Butanol	50	10	0.5	3200	0.24	13000	12,000
	IPA			0.6	1300	0.29	4600	5600
HCl-treated BTESE [173]	Acetic acid	80	10	2.05	2900	9.85	290	780
Spray-coated BTESE [44]	Ethanol	105	10	5.9	1200	-	-	30
	IPA			5.7	1300	1.7	770	1000
Water plasma-treated MTES [27]	Ethanol	50	10	1.18	2100	4.09-0.69	520-3000	2900
	IPA			1.77	4000	-	>10,000	>10,000
Zr-doped TEOS [174]	IPA	70	10	4.9	4300	5.5	777	2800
Co-doped TEOS [175]	Ethanol	70	5.9	0.8	550	2.7	200	1675

Organosilica membranes derived from BTESE (a major component of ECN and HybSi® membranes) are widely investigated to dehydrate solvents, such as ethanol [23, 168], IPA [174], butanol [56, 85], and acetic acid [173, 176], because of their strong resistance to hydrothermal degradation and tunable porous structures. For example, increasing the AR from 0.01 to 1 increased the pore size from 0.44 to 0.54 nm and thus water permeance from 1300 to 2700 GPU but decreased water/IPA selectivity from 4600 to 930 at 50 °C with the feed containing 10 wt% water [58]. On the other hand, post-synthesis exposure of the BTESE membrane to HCl vapor promoted condensation of silanol groups, inducing tighter network structure [173]. Specifically, the HCl vapor exposure improved water/acetic acid selectivity from 130 to 290 and only slightly decreased water permeance from 3400 to 2900 GPU [173]. The BTESE sol can also be coated on porous polysulfone support via spray-coating, and the membrane exhibited water permeance of 1300 GPU and water/IPA selectivity of 770 [44].

Improving silica membrane hydrophilicity is another effective approach to achieving attractive pervaporation performance. For example, MTES/BTESE membranes were treated using atmospheric water plasma followed by low-temperature annealing [27]. Fig. 19a presents the schematic of the structural changes in these two steps. The plasma treatment formed hydrophilic/hydrophobic nano-gradient along membrane pores, as shown by the increased water contact angle as a function of the membrane depth (Fig. 19b). Both water flux and water/solvent selectivity increased because of the enhanced hydrophilicity and pore tightening (Fig. 19c). The water-plasma treated MTES/BTESE exhibited highly crosslinked networks with pore sizes of ~0.4 nm and water permeance of 2000 - 4000 GPU (Fig. 19d). Such membranes showed water/ethanol selectivity of 520 – 3100 and water/IPA selectivity of >10,000.

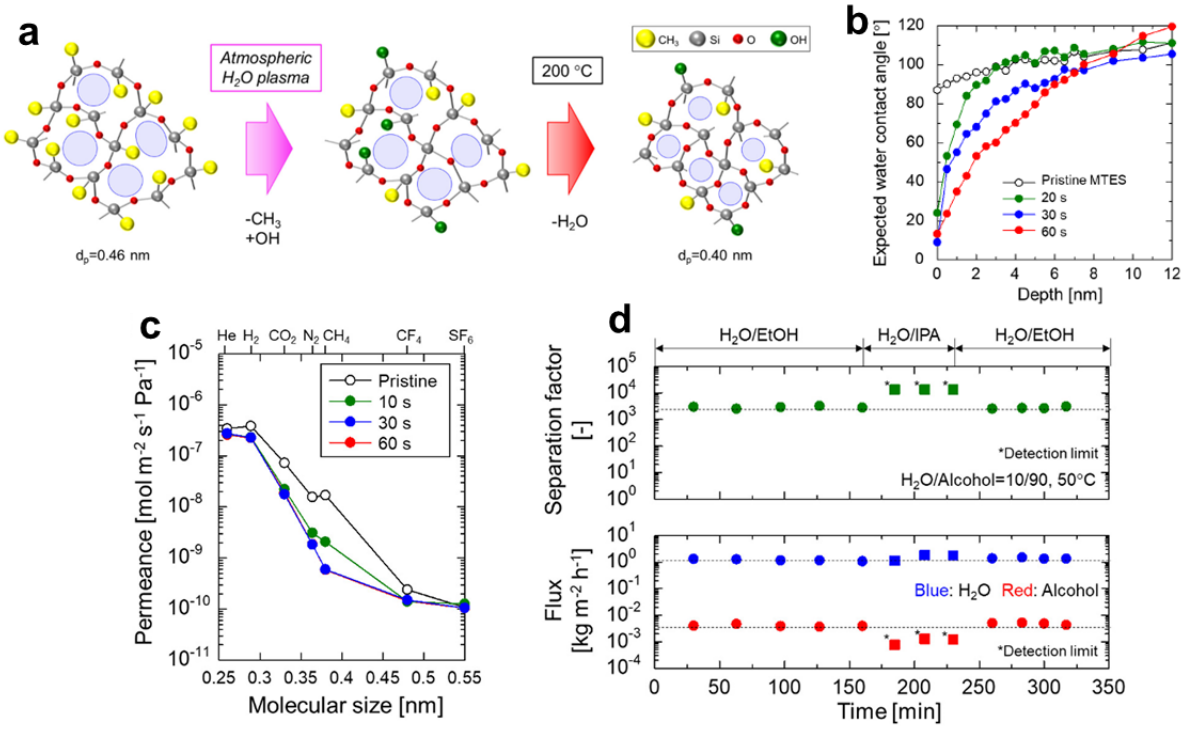

Fig. 19. (a) Schematic of membrane structural changes after the water plasma treatment and annealing. (b) Expected water contact angle at different membrane depth. (c) Pure-gas permeance of pristine and plasma-treated MTES/BTESE membrane. (d) Water/alcohol separation factor and water flux as a function of operation time. Copyright (2022) American Chemical Society [27].

6.2. Desalination

6.2.1 Reverse osmosis desalination

Reverse osmosis (RO) has emerged as a dominant technology to desalinate salty water, as it uses pressure as the driving force for water permeation without phase change. Polyamides (PAs) are the state-of-the-art membrane with water permeance of 1 - 2 L m^{-2} h^{-1} bar^{-1} (LMH/bar) and high NaCl rejection (> 99%) [177, 178]. However, PAs can be degraded by chlorine solutions used for disinfection and fouled by contaminants in feed solutions [179, 180]. By contrast, silica membranes have good chemical resistance and controllable pore sizes (3-5 Å), rendering good potential to selectively permeate water (d_k = 2.6 Å) and reject hydrated ions, such as Na^+ (7.2 Å) and Cl^- (6.6 Å) [46, 181]. For example, BTESE membranes exhibited NaCl

rejection of > 98% and withstood chlorine exposure of 35,000 ppm h [182]. However, silica membranes often exhibited water flux one to two orders of magnitude lower than the PA membranes because of the smaller pores, greater hydrophobicity, and thicker selective layers. Particularly, the silica layers are 1 μm or above to avoid defects, while the PA layers are usually < 0.2 μm.

To achieve loose porous structures and great hydrophilicity to improve water permeance, organoalkoxysilanes with rigid and hydrophilic bridging units have been developed, such as acetoxy [183], norbornane [130], oxalylure [131], and dioxane [129]. The resultant membranes (Table 1) exhibited looser pore structure, greater hydrophilicity and thus higher water permeance than BTESE with ethane bridging units. For example, organosilica membranes prepared with oxalylure [131] and dioxane [129] bridging units exhibited water permeance of 0.118 and 0.066 LMH/bar, respectively, higher than BTESE (0.036 LMH/bar) [184]. However, the enhanced water permeance was often compromised by the decreased salt rejection. For instance, NaCl rejection was ~ 98% in BTESE [184], but only 85.6% in BTES-MOU [131] and 98.5% in BTES-ED [129].

Another strategy to improve water permeance is to blend the precursors with alkoxysilanes containing hydrophilic groups. For example, (3-glycidyloxypropyl)silane (TEGPS) with hydrophilic epoxy groups was blended with BTESPA to yield hydrophilic membranes with water permeance of 0.35 LMH/bar and NaCl rejection of 97.5% for 2000 ppm salt solution [185]. The enhanced water permeance was attributed to the ring opening of epoxy with amine groups on BTESPA, which hydrolyzed to yield -OH groups. Furthermore, the C-O-Si can be hydrolyzed to generate -OH groups, enhancing water affinity and permeance (Fig. 20a). Similar hydrolysis behavior was observed for BTESE and BTESEthy blended with

hydroxymethyl(triethoxy)silane (HMTES) [186]. Additionally, hydrophilic water channels were successfully achieved for blends of BTESPA and N-(2-hydroxyethyl)-N′-[3-(triethoxysilyl)propyl]urea (HETESPU) (Fig. 20d). The membrane exhibited stable water permeance of 0.67 LMH/bar and NaCl rejection > 95% at 25 – 60 °C for 20 h (Fig. 20e) [70].

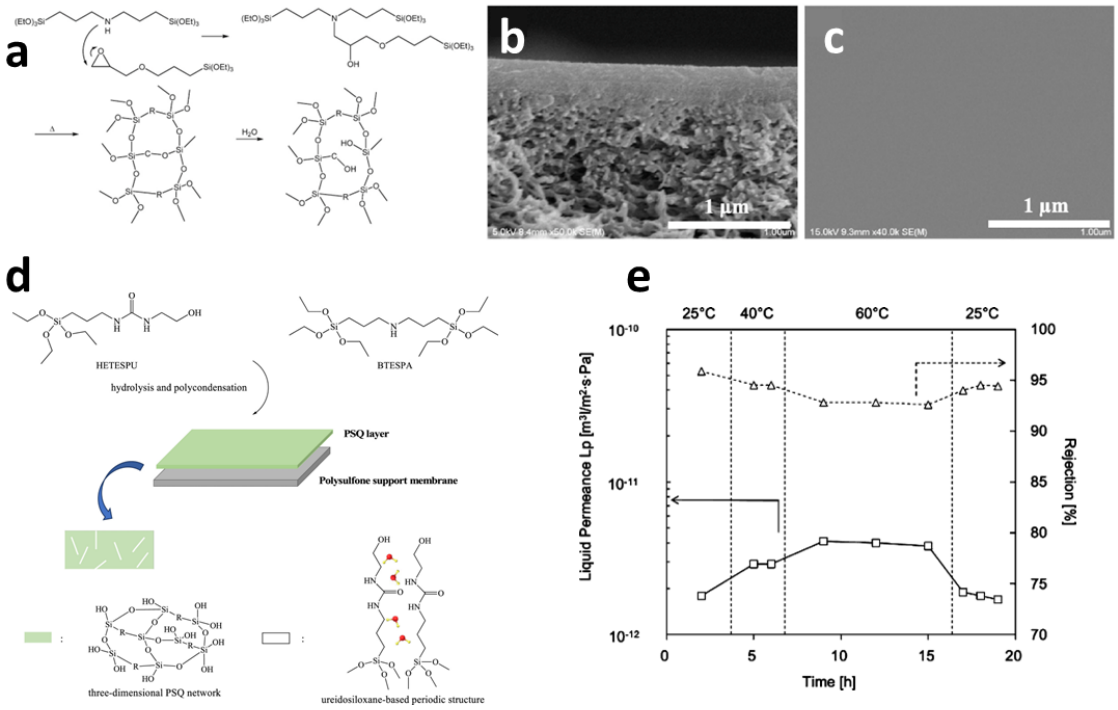

Fig. 20. (a) Schematic for epoxy ring opening and hydrolysis of C-O-Si linkage to generate -OH groups in TEGPS/BTESPA membranes. (b) Cross-sectional and (c) surface SEM of TEGPS/BTESPA membranes. Copyright (2021) Elsevier [185]. (d) Schematic of fabrication of HETESPU/BTESPA membranes providing hydrophilic channels. (e) Desalination performance of HETESPU/BTESPA membranes at different temperatures over time. Copyright (2022) American Chemical Society [70].

6.2.2 Pervaporation desalination

Organosilica membranes have also been investigated for desalination application via pervaporation. As it only vaporizes a portion of water on the permeate side, this process has high energy efficiency and very high salt rejection. Table 6 highlights the silica membranes with attractive pervaporation desalination performance.

Table 6

Structural properties and performance of silica membranes for pervaporation desalination.

Membrane materials	Membrane structure			NaCl (wt%)	Temp. (°C)	Separation properties		
	Surface area (m^2 g^{-1})	Pore size (nm)	Porosity (cm^3/g)			Water flux (kg/m^2 h)	A_W (10^4 GPU)	NaCl rejection (%)
Pristine membranes								
TEOS (RTP) [187]	--	--	--	15	22	0.93	29	> 99
ES40 (RTP) [188]	440-700	2-3	--	3.5	25	2.5	64	~99
BTESE [189]	470	0.3	0.17	0.2	25-70	6 - 18	140 - 46	> 98
BTESEthy [190]	490	0.6	0.32	0.35	70	4.8	13	> 99.5
Metal doping								
Co - TEOS [191]	--	1.7	--	1	20	0.4	14	~ 99.9
Ni - TEOS [192]	100-400	~ 2	--	0.3	60	6	24	~ 99.9
La/Y – BTESE [193]	140-190	0.6	0.06	3.5	25	10.1	260	> 99.9
Carbonized template								
P123/TEOS [181]	1079	3.1	0.89	3.5	22	2.5	77	99.8
				7.5	60	6.6	27	99.9
P123/ES40 [194]	672	3.7	0.45	0.3	25	6.2	159	99.8
				1		4.9	125	99.8
P123/VTES [195]	554	2.7	0.38	1-15	60-25	5.7-2.7	23–69	> 99.7
P123/VTES-TEOS [196]	760	2	0.6	3.5	25	9.5	240	> 98
PEG-PPG-PEG/TEOS [197]	837	1.15	0.48	0.3	60	3.7	15	98.5
Glucose/TEOS [198]	-	-	-	7.5	25	1.8	46	99.5
Pectin /TEOS [199]	-	-	-	-	60	30	120	99.3
Carbonized silica [200]	-	-	-	0.3-3.5	20	2.1-1.9	73-66	> 99

Calcination conditions can be optimized to manipulate silica structures and thus desalination performance. For instance, calcination temperature for BTESE membranes can be adjusted to achieve water permeance ranging from 5×10^5 to 14×10^5 GPU and salt rejection >98% [189]. Additionally, rapid thermal process (RTP) was employed for ES40 over conventional thermal process (CTP) to improve the performance. Fig. 21a,b presents the surface and cross-sectional SEM images of interlayer-free ES40 membranes prepared from RTP, respectively. RTP resulted in a higher surface area and larger pore volume than CTP (Fig. 21c) regardless of the pH values of the sol solutions [188]. Moreover, RTP provided higher content of hydrophilic silanol groups than CTP, increasing water permeance (Fig. 21d) [188]. Specifically, the membranes prepared from RTP exhibited water permeance of 72×10^4 GPU and salt rejection of > 99% for 3.5 wt% salt solutions at 60 °C [188].

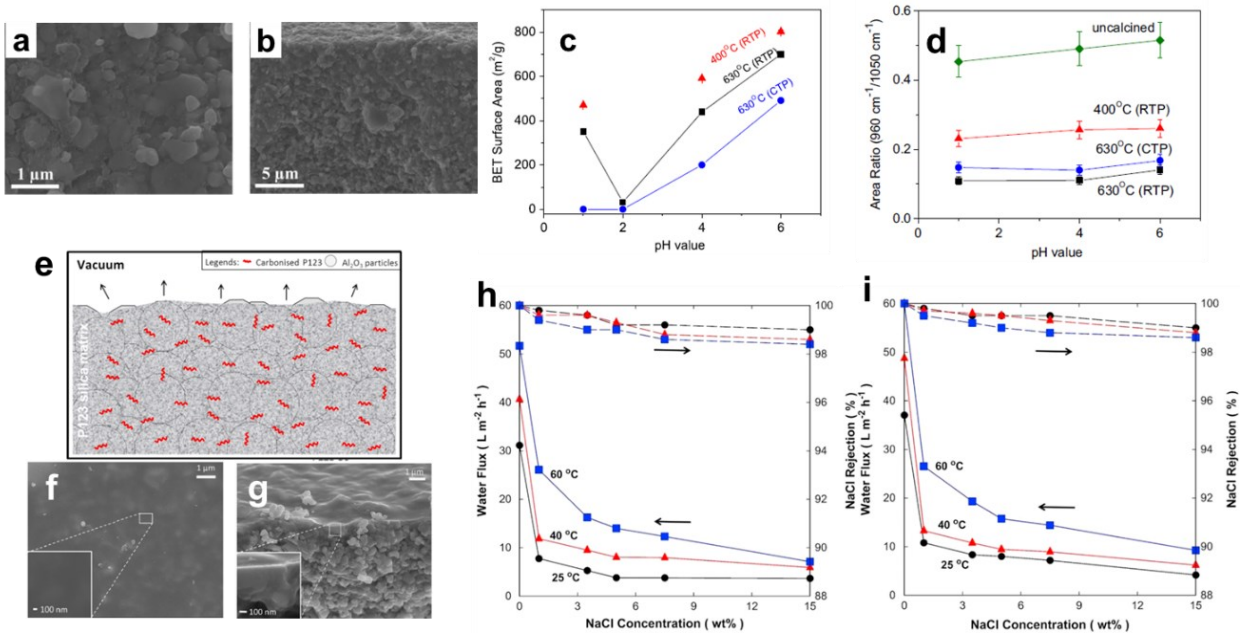

Fig. 21 (a) Surface and (b) cross-sectional SEM images of interlayer-free ES40 prepared from RTP. (c) BET surface area and (d) the ratio of silanol (960 cm^{-1})/siloxane (1050 cm^{-1}) of ES40 membranes prepared using RTP and CTP at different pH values. Copyright (2016) Elsevier [188]. (e) Schematic, (f) surface SEM image, and (g) cross-sectional SEM image of TEOS membranes with P123 carbonized template. Copyright (2014) Elsevier [181]. Pervaporation performance at different salt concentrations and temperatures of (h) N_2 calcinated and (i) vacuum calcinated P123 carbonized template VTES/TEOS. Copyright (2016) Elsevier [196].

Water permeance of silica membranes can be improved by reducing the transport resistance in the interlayer, though it might induce defects and lower salt rejection [181, 196]. To address this issue, carbonized template technique was developed by incorporating organic moieties into the sols before the coating [196]. Fig. 21e presents the schematic of P123 incorporated interlayer-free TEOS membranes. Increasing the P123 content from 5 to 50 wt% increased the surface area from 588 to 1079 m^2 g^{-1}, the pore size from 1.79 to 3.1 nm, the pore volume from 0.23 to 0.89 cm^3 g^{-1}, and water permeance from 11×10^4 to 27×10^4 GPU while maintaining the salt rejection of > 99% [181]. Furthermore, the carbonized template increased hydrothermal stability, which was unusual for TEOS-derived materials. The incorporation of P123 also improved water permeance while maintaining the high salt rejection in ES40 [194] and VTES/TEOS blends [196]. Other organic moieties, such as glucose [198] and Pectin [199], have also been investigated as carbon sources.

6.3 Organic solvent separation

Organosilica membranes have also emerged as a promising platform for organic solvent separation due to their excellent chemical stability [166] and great tunability of pore size and chemistries derived from the pendant and bridged organic groups. For instance, BTESA membranes with rigid acetylene linkages were explored for the separation of methanol from organic solvents in both pervaporation and RO modes. Fig. 22a presents the SEM cross-sectional image of BTESA membranes prepared on α-Al_2O_3 support with SiO_2-ZrO_2 interlayer. The membranes exhibited excellent pervaporation separation of methanol from methyl acetate, butyl acetate, and butanol (Fig. 22b) because of the uniform pore size of BTESA (0.4 - 0.5 nm) and preferable methanol sorption [201]. In addition, BTESA membranes were also studied to

separate methanol from dimethyl carbonate [201], ethanol, isopropanol, and toluene [202, 203]. Moreover, the BTESA membranes showed excellent stability for methanol/methyl tert-butyl ether separation using RO (Fig. 22c) and great resistance to aging (Fig. 22d) [204].

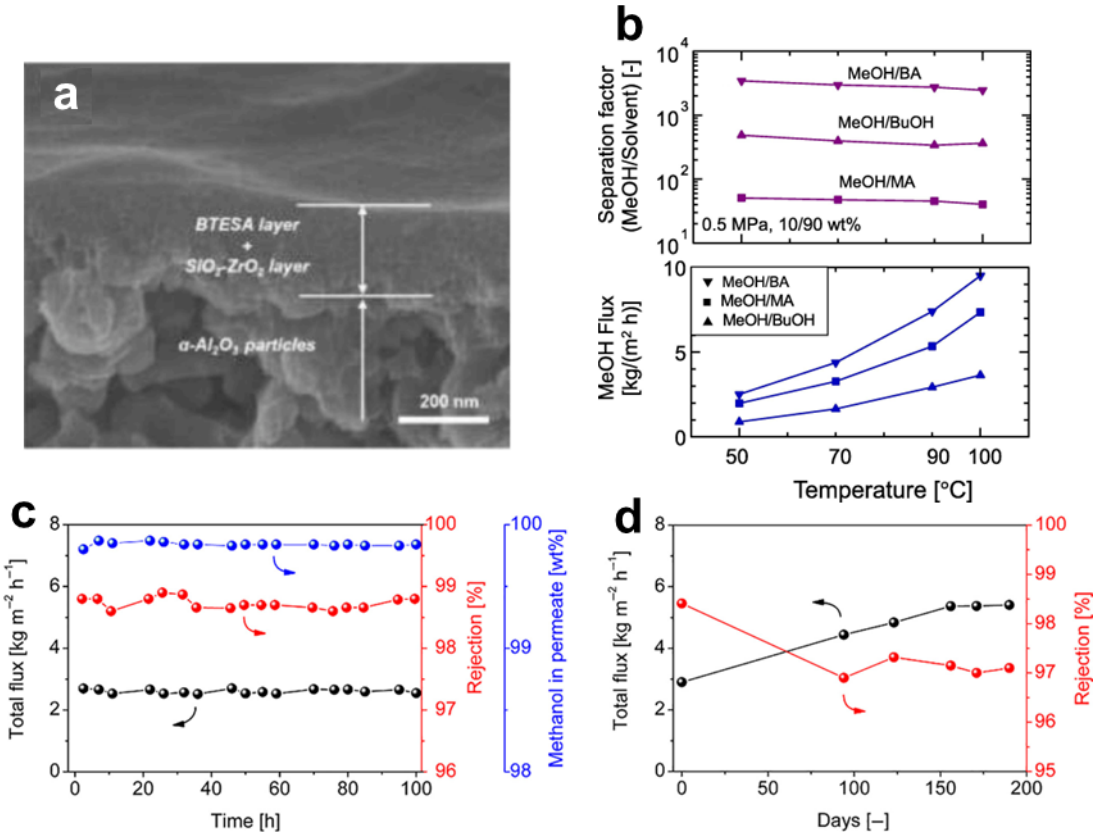

Fig. 22. (a) Cross-sectional SEM image of BTESA membrane. Copyright (2020) Elsevier [201]. (b) Pervaporation performance of BTESA as a function of temperature. Copyright (2022) Elsevier [203]. (c) Continuous RO operation and (d) long-term stability of BTESA membranes for methanol/methyl tert-butyl ether separation. Copyright (2022) American Institute of Chemical Engineers [204].

7. Silica membrane reactors

Silica membranes are explored for membrane reactors combining catalytic reaction and molecular separation in one step to improve product conversion and lower costs. For example, commercial HybSi® membranes were used to produce 1,1-diethoxybutane from the acetalization of butyraldehyde and ethanol by selectively removing water byproduct and shifting the

acetalization [30-32]. The membranes improved the acetalization conversion to 70% from the thermodynamic limit of 40% at 70 °C [32]. A technoeconomic analysis showed that the membrane reactor lowered the acetal production cost by 40% [30]. Pervatech membranes were also investigated to produce ethyl lactate by removing water [205-208], obtaining ethyl lactate conversion of 98% at a purity of 96% [206] while reducing ethanol consumption by ~60% (compared with conventional pack bed reactors) [205].

Organosilica membranes can also remove methanol to promote transesterification, such as production of butyl acetate [202, 203]. For instance, batch-type BTESA membrane reactors improved butyl acetate yield from 60% to 95.4% because of the high methanol permeance (3200 GPU) and excellent methanol/butyl acetate separation factor (210) [202].

Silica membrane reactors have also been used to promote H_2 production due to their excellent H_2/gas separation properties [209], such as water-gas shift reaction [210], methanol reforming [211], and hydrogen iodide (HI) decomposition [212, 213]. For example, HMDSO-derived silica membranes were used for water-gas shift reaction, demonstrating CO conversion of 95-97%, H_2 purity of 94%, and H_2 recovery of 60% at 300 °C [210]. Additionally, TEOS-derived membranes for MeOH reforming increased MeOH conversion by 15% and H_2 yield by 10% [211]. The use of hexyltrimethoxysilane (HTMOS) derived tubular membranes increased HI conversion from 20% to 60% because of their high H_2 permeance of 930 GPU and H_2/N_2 selectivity of 160 [213]. On the other hand, the use of BTESE-derived membranes increased the conversion of methylcyclohexane (MCH) dehydrogenation from 44% to 86% while producing H_2 with a purity of 99.9% [214, 215].

8. Conclusion and perspectives

This review aims to capture the exciting advancement of silica membranes, focusing on novel fabrication methods to enhance scalability and new chemistries and structures to improve separation properties and hydrothermal stabilities. Conventional silica membranes can be prepared using sol-gel and have been practiced for industrial solvent dehydration. Various methods have been developed to produce silica membranes at low temperatures, such as PE-CVD and plasma oxidation process. Particularly, oxygen plasma treatment of polysiloxanes renders a rapid and scalable way to fabricate thin silica membranes with superior H_2/CO_2 separation performance. A variety of strategies have been developed to improve hydrothermal stability and molecular sieving ability by molecular engineering of precursors, precursor blending, metal doping, and incorporation with nanofillers. The silica membranes have also been explored for a variety of separations (such as H_2/CO_2, H_2/CH_4, CO_2/N_2, and C_3H_6/C_3H_8) and membrane reactors for H_2 production and esterification.

We optimistically expect that silica membranes will continue their upward trajectory toward practical applications. First, silica membranes are well-positioned for H_2/CO_2 and H_2/CH_4 separation at elevated temperatures, which is critical to enable large-scale H_2 production and delivery with minimal environmental impact. Second, newly developed scalable processes to fabricate membranes with thin silica layers at low temperatures can be expanded for other precursors, lowering the costs of large-scale production and enabling industrial applications. Third, silica membranes show great promise for solvent separations by pervaporation or RO because of their excellent resistance to chemicals and heat. Finally, silica membranes hold great potential for membrane reactors to achieve process intensification to lower production costs as they can remove small byproducts (such as H_2, H_2O, methanol, etc.) to shift the reactions.

Declaration of competing interest

There are no conflicts to declare.

Acknowledgments

We acknowledge the financial support from the U.S. National Science Foundation (# 2044623).

Abbreviation	Full name
AP-PECVD	atmospheric pressure – plasma-enhanced chemical vapor deposition
AR	acid molar ratio (mole of acid / mole of alkoxysilane)
CTP	conventional thermal process
CVD	chemical vapor deposition
FAV	fractional accessible volume
GO	graphene oxide
GPU	gas permeation unit
h-pcff	hybrid polymer consistent force-field
mGT	modified gas translation
MMMs	mixed matrix materials
NEMD	nonequilibrium molecular dynamics
NKP	normalized Knudsen permeation
pcff	polymer consistent force-field
PE-CVD	plasma-enhanced chemical vapor deposition
RTP	rapid thermal process
r-GO	reduced graphene oxide
SD	solution diffusion
SEM	scanning electron microscopy
SR	solvent molar ratio (mole of solvent/ mole of alkoxysilane)
STP	Standard temperature and pressure
SW-BMH	Stillinger Weber three-body interactions and modified Born–Mayer–Huggins pair potential
WR	water molar ratio (mole of water/ mole of alkoxysilane)
WSG	water gas shift
Chemical	
APTES	(3-aminopropyl)triethoxysilane

BTESA	1,2-bis(triethoxysiyl)acetylene
BTES-Ac	1,6-diacetoxy-3,4-bis(triethoxysilyl)hexa-2,4-diene
BTESB	bis(triethoxysilyl)benzene
BTESBPh	4,4′ -bis(triethoxysilyl)-1,1′ -biphenyl
BTESE	1,2-bis(triethoxysiyl)ethane
BTES-ED	2,5-bis[2 -(triethoxysilyl)ethyl]-1,4-dioxane
BTESEthyl	1,2-bis(triethoxysiyl)ethylene
BTESM	bis(triethoxysilyl)methane
BTES-MAz	1,4-bis(triethoxysilylmethyl)-1,2,3-triazole
BTES-MOU	bis(triethoxysilylmethyl)-N,N′-oxalylureas
BTESO	bis(triethoxysilyl)octane
BTESP	1,2-bis(triethoxysilyl)propane
BTESPA	bis[3-(triethoxysilyl)propyl]amine
BTES-POU	bis(triethoxysilylmpropyl)-N,N′-oxalylureas
BTMSH	bis(trimethoxysilyl)hexane
BTMS-Nor	bis(trimethoxysilyl)norbornane
BTPP	4,6-bis(3-triethoxysilyl-1-propoxy)-1,3-pyrimidine
DMDMOS	dimethyldimethoxysilate
DMDMS	dimethyldimethylsilane
DPhDMOS	diphenyldimethoxysilane
EtOH	ethanol
HETESPU	N-(2-hydroxyethyl)-N′-[3-(triethoxysilyl)propyl] urea
HETESPU	N-(2-hydroxyethyl)-N′-[3-(triethoxysilyl)propyl]urea
HI	hydrogen iodide
HMDSO	hexamethyldisiloxane
HMTES	hydroxymethyl(triethoxy)silane
MCH	methylcyclohexane
MTES	methyltriethoxysilane
MTMOS	methyltrimethoxysilane
NMP	N-methyl pyrrolidone
PA	polyamide
PA-Si	3-(triethoxysilyl)propan-1-amine
PDMS	polydimethylsiloxane
PEG-PPG-PEG	polyethylene glycol-polypropylene glycol-polyethylene glycol
PES	polyethersulfone
PhTES	phenyltriethoxysilane
PhTMOS	phenyltrimethoxysilane
POSS	polyhedral oligomeric silsesquioxane
PSF	polysulfone
SA-Si	3-(triethoxysilyl)-N-methylpropan-1-amine

TA-Si	3-(triethoxysilyl)-N,N-dimethylpropan-1-amine
TEFS	triethoxyfluorosilane
TEGPS	(3-glycidyloxypropyl)silane
TEOS	tetraethyl orthosilicate
THF	tetrahydrofuran
TMOS	tetramethyl orthosilicate
TPMS	triphenylmethoxysilane
TRIES	triethoxysilane
VTES	vinyltriethoxysilane
VTMS	vinyltrimethoxysilane

Mathematics

d_i	penetrant kinetic diameter
d_p	membrane pore diameter
D	diffusivity
D_0	pre-exponential factor of diffusivity
$E_{D,i}$	activation energy for diffusion for gas *i*
$E_{D,SD}$	activation energy for diffusion for the SD model in Eq. 3
E_P	activation energy for permeation
f_{NKP}	Normalized Knudsen Permeance
ΔH_S	enthalpy of sorption
$k_{0,i}$	geometric value
L	silica thickness
M_i	penetrant molar mass
P	gas permeability
P_o	pre-exponential factor of permeability
Q	gas permeance
R	universal gas constant
S	gas solubility
S_0	pre-exponential factor of solubility
T	absolute temperature (in Kelvin)
ε	membrane porosity
ρ	diffusional probability
τ	tortuosity

References

[1] H. Park, J. Kamcev, L. M. Robeson, M. Elimelech, B. D. Freeman. Maximizing the right stuff: The trade-off between membrane permeability and selectivity. Science. 356 (2017) eaab0530, 10.1126/science.aab0530.

[2] W. J. Koros, C. Zhang. Materials for next-generation molecularly selective synthetic membranes. Nat. Mater. 16 (2017) 289-297, 10.1038/nmat4805.
[3] M. Galizia, W. S. Chi, Z. P. Smith, T. C. Merkel, R. W. Baker, B. D. Freeman. 50th Anniversary perspective: Polymers and mixed matrix membranes for gas and vapor separation: A review and prospective opportunities. Macromolecules. 50 (2017) 7809-7843, 10.1021/acs.macromol.7b01718.
[4] G. Chen, T. Wang, G. Zhang, G. Liu, W. Jin. Membrane materials targeting carbon capture and utilization. Adv. Membr. 2 (2022) 100025, 10.1016/j.advmem.2022.100025.
[5] L. Hu, S. Pal, H. Nguyen, V. Bui, H. Lin. Molecularly engineering polymeric membranes for H_2/CO_2 separation at 100–300° C. J. Polym. Sci. 58 (2020) 2467-2481, 10.1002/pol.20200220.
[6] Y. Liu, Y. Ren, H. Ma, G. He, Z. Jiang. Advanced organic molecular sieve membranes for carbon capture: Current status, challenges and prospects. Adv. Membr. 2 (2022) 100028, 10.1016/j.advmem.2022.100028.
[7] L. Hu, K. Clark, T. Alebrahim, H. Lin. Mixed matrix membranes for post-combustion carbon capture: From materials design to membrane engineering. J. Membr. Sci. 644 (2022) 120140, 10.1016/j.memsci.2021.120140.
[8] Y. Han, W. W. Ho. Polymeric membranes for CO_2 separation and capture. J. Membr. Sci. 628 (2021) 119244, 10.1016/j.memsci.2021.119244.
[9] S. Chisca, V.-E. Musteata, W. Zhang, S. Vasylevskyi, G. Falca, E. Abou-Hamad, A.-H. Emwas, M. Altunkaya, S. P. Nunes. Polytriazole membranes with ultrathin tunable selective layer for crude oil fractionation. Science. 376 (2022) 1105-1110, 10.1126/science.abm7686.
[10] H. Zeng, S. He, S. S. Hosseini, B. Zhu, L. Shao. Emerging nanomaterial incorporated membranes for gas separation and pervaporation towards energetic-efficient applications. Adv. Membr. 2 (2022) 100015, 10.1016/j.advmem.2021.100015.
[11] H. Lin, M. Yavari. Upper bound of polymeric membranes for mixed-gas CO_2/CH_4 separations. J. Membr. Sci. 475 (2015) 101-109.
[12] I. Rana, H. Nagasawa, K. Yamamoto, T. Gunji, T. Tsuru, M. Kanezashi. Effect of fluorine doping on the network pore structure of non-porous organosilica bis(triethoxysilyl)propane (BTESP) membranes for use in molecular separation. J. Membr. Sci. 644 (2022) 120083, 10.1016/j.memsci.2021.120083.
[13] G. Dong, H. Nagasawa, L. Yu, M. Guo, M. Kanezashi, T. Yoshioka, T. Tsuru. Energy-efficient separation of organic liquids using organosilica membranes via a reverse osmosis route. J. Membr. Sci. 597 (2020) 117758, 10.1016/j.memsci.2019.117758.
[14] L. Zhu, L. Huang, S. R. Venna, A. K. Blevins, Y. Ding, D. P. Hopkinson, M. T. Swihart, H. Lin. Scalable polymeric few-nanometer organosilica membranes with hydrothermal stability for selective hydrogen separation. ACS Nano. (2021) 12119–12128, 10.1021/acsnano.1c03492.
[15] T. Tsuru. Silica-based membranes with molecular-net-sieving properties: Development and applications. J. Chem. Eng. Japan. 51 (2018) 713-725, 10.1252/jcej.17we235.
[16] H.-J. Kim, W. Chaikittisilp, K.-S. Jang, S. A. Didas, J. R. Johnson, W. J. Koros, S. Nair, C. W. Jones. Aziridine-functionalized mesoporous silica membranes on polymeric hollow fibers: Synthesis and single-component CO_2 and N_2 permeation properties. Ind. Eng. Chem. Res. 54 (2015) 4407-4413, 10.1021/ie503781u.

[17] M. Kanezashi, T. Shioda, T. Gunji, T. Tsuru. Gas permeation properties of silica membranes with uniform pore sizes derived from polyhedral oligomeric silsesquioxane. AIChE J. 58 (2012) 1733-1743, 10.1002/aic.12716.
[18] K.-S. Jang, H.-J. Kim, J. R. Johnson, W.-g. Kim, W. J. Koros, C. W. Jones, S. Nair. Modified mesoporous silica gas separation membranes on polymeric hollow fibers. Chem. Mater. 23 (2011) 3025-3028, 10.1021/cm200939d.
[19] H. Qi, J. Han, N. Xu, H. J. Bouwmeester. Hybrid organic–inorganic microporous membranes with high hydrothermal stability for the separation of carbon dioxide. ChemSusChem. 3 (2010) 1375-1378, 10.1002/cssc.201000242.
[20] M. Kanezashi, K. Yada, T. Yoshioka, T. Tsuru. Organic–inorganic hybrid silica membranes with controlled silica network size: preparation and gas permeation characteristics. J. Membr. Sci. 348 (2010) 310-318, 10.1016/j.memsci.2009.11.014.
[21] Y. Ohta, K. Akamatsu, T. Sugawara, A. Nakao, A. Miyoshi, S.-I. Nakao. Development of pore size-controlled silica membranes for gas separation by chemical vapor deposition. J. Membr. Sci. 315 (2008) 93-99, 10.1016/j.memsci.2008.02.008.
[22] H. M. Van Veen, Y. C. Van Delft, C. W. R. Engelen, P. P. A. C. Pex. Dewatering of organics by pervaporation with silica membranes. Sep. Purif. Technol. 22 (2001) 361-366, 10.1016/S1383-5866(00)00119-2.
[23] R. Kreiter, M. D. A. Rietkerk, H. L. Castricum, H. M. van Veen, J. E. ten Elshof, J. F. Vente. Evaluation of hybrid silica sols for stable microporous membranes using high-throughput screening. J. Solgel Sci. Technol. 57 (2011) 245-252, 10.1007/s10971-010-2208-7.
[24] T. Gallego-Lizon, E. Edwards, G. Lobiundo, L. Freitas dos Santos. Dehydration of water/t-butanol mixtures by pervaporation: comparative study of commercially available polymeric, microporous silica and zeolite membranes. J. Membr. Sci. 197 (2002) 309-319, 10.1016/S0376-7388(01)00650-0.
[25] A. M. Urtiaga, C. Casado, I. Ortiz. Pervaporative dehydration of an industrial ketonic solvent using ceramic silica membranes. Mater. Res. Soc. Symp. Procy. 752 (2003) 116, 10.1557/PROC-752-AA11.6.
[26] S. Sommer, T. Melin. Performance evaluation of microporous inorganic membranes in the dehydration of industrial solvents. Chem. Eng. Process. 44 (2005) 1138-1156, 10.1016/j.cep.2005.02.006.
[27] S. Aoyama, H. Nagasawa, M. Kanezashi, T. Tsuru. Nanogradient hydrophilic/hydrophobic organosilica membranes developed by atmospheric-pressure plasma to enhance pervaporation performance. ACS Nano. 16 (2022) 10302-10313, 10.1021/acsnano.1c11656.
[28] A. Rajawat, S. Subramanian, S. Ramakrishna. Progress on silica pervaporation membranes in solvent dehydration and solvent recovery processes. Materials. 13 (2020) 3354, 10.3390/ma13153354.
[29] X. Ren, T. Tsuru. Organosilica-based membranes in gas and liquid-phase separation. Membranes. 9 (2019) 107, 10.3390/membranes9090107.
[30] I. Agirre, M. B. Güemez, A. Motelica, H. M. van Veen, J. F. Vente, P. L. Arias. A techno‐economic comparison of various process options for the production of 1, 1‐diethoxy butane. J. Chem. Technol. Biotechnol. 87 (2012) 943-954, 10.1002/jctb.3704.

[31] I. Agirre, M. B. Güemez, A. Motelica, H. M. van Veen, J. F. Vente, P. L. Arias. The conceptual design of a continuous pervaporation membrane reactor for the production of 1, 1 - diethoxy butane. AIChE J. 58 (2012) 1862-1868, 10.1002/aic.12692.

[32] I. Agirre, M. Güemez, H. van Veen, A. Motelica, J. Vente, P. Arias. Acetalization reaction of ethanol with butyraldehyde coupled with pervaporation. Semi-batch pervaporation studies and resistance of HybSi® membranes to catalyst impacts. J. Membr. Sci. 371 (2011) 179-188, 10.1016/j.memsci.2011.01.031.

[33] S. J. Khatib, S. T. Oyama. Silica membranes for hydrogen separation prepared by chemical vapor deposition (CVD). Sep. Purif. Technol. 111 (2013) 20-42, 10.1016/j.seppur.2013.03.032.

[34] J. Sunarso, S. S. Hashim, Y. S. Lin, S. M. Liu. Membranes for helium recovery: An overview on the context, materials and future directions. Sep. Purif. Technol. 176 (2017) 335-383, 10.1016/j.seppur.2016.12.020.

[35] M. Guo, M. Kanezashi. Recent progress in a membrane-based technique for propylene/propane separation. Membranes. 11 (2021) 310, 10.3390/membranes11050310.

[36] L. Yu, M. Kanezashi, H. Nagasawa, T. Tsuru. Role of amine type in CO_2 separation performance within amine functionalized silica/organosilica membranes: a review. Appl. Sci. 8 (2018) 1032, 10.3390/app8071032.

[37] A. Kayvani Fard, G. McKay, A. Buekenhoudt, H. Al Sulaiti, F. Motmans, M. Khraisheh, M. Atieh. Inorganic membranes: Preparation and application for water treatment and desalination. Materials. 11 (2018) 74, 10.3390/ma11010074.

[38] R. M. De Vos, H. Verweij. High-selectivity, high-flux silica membranes for gas separation. Science. 279 (1998) 1710-1711, 10.1126/science.279.5357.1710.

[39] L. Hu, V. T. Bui, A. Krishnamurthy, S. Fan, W. Guo, S. Pal, X. Chen, G. Zhang, Y. Ding, R. P. Singh. Tailoring sub-3.3 Å ultramicropores in advanced carbon molecular sieve membranes for blue hydrogen production. Sci. Adv. 8 (2022) eabl8160, 10.1126/sciadv.abl8160.

[40] M. Kanezashi, T. Matsutani, H. Nagasawa, T. Tsuru. Fluorine-induced microporous silica membranes: Dramatic improvement in hydrothermal stability and pore size controllability for highly permeable propylene/propane separation. J. Membr. Sci. 549 (2018) 111-119, 10.1016/j.memsci.2017.11.072.

[41] G. Gong, H. Nagasawa, M. Kanezashi, T. Tsuru. Tailoring the separation behavior of polymer-supported organosilica layered-hybrid membranes via facile Post-treatment using HCl and HNO_3 vapors. ACS Appl. Mater. Interfaces. 8 (2016) 11060-11069, 10.1021/acsami.6b01986.

[42] N. W. Ockwig, T. M. Nenoff. Membranes for hydrogen separation. Chem. Rev. 107 (2007) 4078-4110, 10.1021/cr0501792.

[43] M. Kawasaki, H. Nagasawa, M. Kanezashi, T. Tsuru. Open-air plasma deposition of polymer-supported silica-based membranes for gas separation. Sep. Purif. Technol. 291 (2022) 120908, 10.1016/j.seppur.2022.120908.

[44] H. Guan, Y. Li, G. Gong, R. Xu, Y. Hu, T. Tsuru. Enhancing dehydration performance of isopropanol for flexible hybrid silica composite membranes with spray-coated active layer on polymers. Sep. Purif. Technol. 283 (2022) 120230, 10.1016/j.seppur.2021.120230.

[45] T. Tsuru. Development of metal-doped silica membranes for increased hydrothermal stability and their applications to membrane reactors for steam reforming of methane. J. Japan Pet. Inst. 54 (2011) 277-286, 10.1627/jpi.54.277.
[46] M. Elma, C. Yacou, D. K. Wang, S. Smart, J. C. Diniz da Costa. Microporous silica based membranes for desalination. Water. 4 (2012), 10.3390/w4030629.
[47] I. Agirre, P. L. Arias, H. L. Castricum, M. Creatore, E. Johan, G. G. Paradis, P. H. Ngamou, H. M. van Veen, J. F. Vente. Hybrid organosilica membranes and processes: Status and outlook. Sep. Purif. Technol. 121 (2014) 2-12, 10.1016/j.seppur.2013.08.003.
[48] C. Milea, C. Bogatu, A. Duta. The influence of parameters in silica sol-gel process. Bull. Transilv. Univ. Bras. 4 (2011) 59-66.
[49] C. J. Brinker. Hydrolysis and condensation of silicates: effects on structure. J. Non-Cryst. Solids. 100 (1988) 31-50, 10.1016/0022-3093(88)90005-1.
[50] C. J. Brinker, G. W. Scherer. Sol→ gel→ glass: I. Gelation and gel structure. J. Non-Cryst. Solids. 70 (1985) 301-322, 10.1016/0022-3093(85)90103-6.
[51] X. Yu, L. Meng, T. Niimi, H. Nagasawa, M. Kanezashi, T. Yoshioka, T. Tsuru. Network engineering of a BTESE membrane for improved gas performance via a novel pH-swing method. J. Membr. Sci. 511 (2016) 219-227, 10.1016/j.memsci.2016.03.060.
[52] D. Wang, G. P. Bierwagen. Sol–gel coatings on metals for corrosion protection. Prog. Org. Coat. 64 (2009) 327-338, 10.1016/j.porgcoat.2008.08.010.
[53] T. Coradin, M. Boissière, J. Livage. Sol-gel chemistry in medicinal science. Curr. Med. Chem. 13 (2006) 99-108, 10.2174/092986706789803044.
[54] T. Niimi, H. Nagasawa, M. Kanezashi, T. Yoshioka, K. Ito, T. Tsuru. Preparation of BTESE-derived organosilica membranes for catalytic membrane reactors of methylcyclohexane dehydrogenation. J. Membr. Sci. 455 (2014) 375-383, 10.1016/j.memsci.2014.01.003.
[55] H. Song, Y. Wei, C. Wang, S. Zhao, H. Qi. Tuning sol size to optimize organosilica membranes for gas separation. Chin. J. Chem. Eng. 26 (2018) 53-59, 10.1016/j.cjche.2017.04.010.
[56] H. L. Castricum, G. G. Paradis, M. C. Mittelmeijer-Hazeleger, W. Bras, G. Eeckhaut, J. F. Vente, G. Rothenberg, E. Johan. Tuning the nanopore structure and separation behavior of hybrid organosilica membranes. Microporous Mesoporous Mater. 185 (2014) 224-234, 10.1016/j.micromeso.2013.11.005.
[57] H. L. Castricum, H. F. Qureshi, A. Nijmeijer, L. Winnubst. Hybrid silica membranes with enhanced hydrogen and CO_2 separation properties. J. Membr. Sci. 488 (2015) 121-128, 10.1016/j.memsci.2015.03.084.
[58] N. Moriyama, H. Nagasawa, M. Kanezashi, T. Tsuru. Pervaporation dehydration of aqueous solutions of various types of molecules via organosilica membranes: Effect of membrane pore sizes and molecular sizes. Sep. Purif. Technol. 207 (2018) 108-115, 10.1016/j.seppur.2018.06.021.
[59] M. Kanezashi, R. Matsugasako, H. Tawarayama, H. Nagasawa, T. Tsuru. Pore size tuning of sol-gel-derived triethoxysilane (TRIES) membranes for gas separation. J. Membr. Sci. 524 (2017) 64-72, 10.1016/j.memsci.2016.11.006.
[60] J.-Y. Li, D. K. Wang, H.-H. Tseng, M.-Y. Wey. Solvent effects on diffusion channel construction of organosilica membrane with excellent CO_2 separation properties. J. Membr. Sci. 618 (2021) 118758, 10.1016/j.memsci.2020.118758.

[61] G. Gong, H. Nagasawa, M. Kanezashi, T. Tsuru. Facile and scalable flow-induced deposition of organosilica on porous polymer supports for reverse osmosis desalination. ACS Appl. Mater. Interfaces. 10 (2018) 14070-14078, 10.1021/acsami.7b19075.

[62] H. Zhang, Y. Wei, S. Niu, H. Qi. Fabrication of Pd-Nb bimetallic doped organosilica membranes by different metal doping routes for H_2/CO_2 separation. Chin. J. Chem. Eng. 36 (2021) 67-75, 10.1016/j.cjche.2020.09.003.

[63] U. Anggarini, H. Nagasawa, M. Kanezashi, T. Tsuru. Structural two-phase evolution of aminosilica-based silver-coordinated membranes for increased hydrogen separation. J. Membr. Sci. 642 (2022) 119962, 10.1016/j.memsci.2021.119962.

[64] H. Nagasawa, S. Odagawa, M. Kanezashi, T. Tsuru. Acid post-treatment of sol-gel-derived ethylene-bridged organosilica membranes and their filtration performances. J. Membr. Sci. 556 (2018) 196-202, 10.1016/j.memsci.2018.03.063.

[65] M. Guo, M. Kanezashi, H. Nagasawa, L. Yu, K. Yamamoto, T. Gunji, T. Tsuru. Fine‐tuned, molecular‐composite, organosilica membranes for highly efficient propylene/propane separation via suitable pore size. AIChE J. 66 (2019) e16850, 10.1002/aic.16850.

[66] X. Ren, K. Nishimoto, M. Kanezashi, H. Nagasawa, T. Yoshioka, T. Tsuru. CO_2 permeation through hybrid organosilica membranes in the presence of water vapor. Ind. Eng. Chem. Res. 53 (2014) 6113-6120, 10.1021/ie404386r.

[67] X. Ren, M. Kanezashi, H. Nagasawa, T. Tsuru. Plasma-assisted multi-layered coating towards improved gas permeation properties for organosilica membranes. RSC Adv. 5 (2015) 59837-59844, 10.1039/c5ra08052e.

[68] N. Moriyama, H. Nagasawa, M. Kanezashi, T. Tsuru. Improved performance of organosilica membranes for steam recovery at moderate-to-high temperatures via the use of a hydrothermally stable intermediate layer. J. Membr. Sci. 620 (2021) 118895, 10.1016/j.memsci.2020.118895.

[69] H. Nagasawa, R. Yasunari, M. Kawasaki, M. Kanezashi, T. Tsuru. Facile low-temperature route toward the development of polymer-supported silica-based membranes for gas separation via atmospheric-pressure plasma-enhanced chemical vapor deposition. J. Membr. Sci. 638 (2021) 119709, 10.1016/j.memsci.2021.119709.

[70] D. Zhang, M. Kanezashi, T. Tsuru, K. Yamamoto, T. Gunji, Y. Adachi, J. Ohshita. Development of highly water-permeable robust PSQ-based RO membranes by introducing hydroxyethylurea-based hydrophilic water channels. ACS Appl. Mater. Interfaces. (2022), 10.1021/acsami.2c01469.

[71] D. Zhang, M. Kanezashi, T. Tsuru, K. Yamamoto, T. Gunji, Y. Adachi, J. Ohshita. Development of robust and high-performance polysilsesquioxane reverse osmosis membranes modified by SiO_2 nanoparticles for water desalination. Sep. Purif. Technol. 296 (2022) 121421, 10.1016/j.seppur.2022.121421.

[72] G. Gong, J. Wang, H. Nagasawa, M. Kanezashi, T. Yoshioka, T. Tsuru. Synthesis and characterization of a layered-hybrid membrane consisting of an organosilica separation layer on a polymeric nanofiltration membrane. J. Membr. Sci. 472 (2014) 19-28, 10.1016/j.memsci.2014.08.030.

[73] G. Gong, M. Mamoru, H. Nagasawa, M. Kanezashi, Y. Hu, T. Tsuru. Vapor-permeation dehydration of isopropanol using a flexible and thin organosilica membrane with high permeance. J. Membr. Sci. 588 (2019) 117226, 10.1016/j.memsci.2019.117226.

[74] W. Wei, S. Xia, G. Liu, X. Gu, W. Jin, N. Xu. Interfacial adhesion between polymer separation layer and ceramic support for composite membrane. AIChE J. 56 (2010) 1584-1592, 10.1002/aic.12086.
[75] R. M. De Vos, W. F. Maier, H. Verweij. Hydrophobic silica membranes for gas separation. J. Membr. Sci. 158 (1999) 277-288, 10.1016/S0376-7388(99)00035-6.
[76] R. M. De Vos, H. Verweij. Improved performance of silica membranes for gas separation. J. Membr. Sci. 143 (1998) 37-51, 10.1016/S0376-7388(97)00334-7.
[77] X. Yu, H. Nagasawa, M. Kanezashi, T. Tsuru. Improved thermal and oxidation stability of bis (triethoxysilyl) ethane (BTESE)-derived membranes, and their gas-permeation properties. J. Mater. Chem. A. 6 (2018) 23378-23387, 10.1039/C8TA07572G.
[78] M. Kanezashi, T. Sasaki, H. Tawarayama, T. Yoshioka, T. Tsuru, S. Bhandarkar. Hydrogen permeation properties and hydrothermal stability of sol-gel-derived amorphous silica membranes fabricated at high temperatures. J. Am. Ceram. Soc. 96 (2013) 2950-2957, 10.1111/jace.12523.
[79] S. Oyama, D. Lee, P. Hacarlioglu, R. Saraf. Theory of hydrogen permeability in nonporous silica membranes. J. Membr. Sci. 244 (2004) 45-53, 10.1016/j.memsci.2004.06.046.
[80] K. Akamatsu, M. Suzuki, A. Nakao, S.-i. Nakao. Development of hydrogen-selective dimethoxydimethylsilane-derived silica membranes with thin active separation layer by chemical vapor deposition. J. Membr. Sci. 580 (2019) 268-274, 10.1016/j.memsci.2019.03.024.
[81] H. Kato, S. B. Lundin, S. J. Ahn, A. Takagaki, R. Kikuchi, S. T. Oyama. Gas separation silica membranes prepared by chemical vapor deposition of methyl-substituted silanes. Membranes. 9 (2019) 144, 10.3390/membranes9110144.
[82] H. Nagasawa, H. Shigemoto, M. Kanezashi, T. Yoshioka, T. Tsuru. Characterization and gas permeation properties of amorphous silica membranes prepared via plasma enhanced chemical vapor deposition. J. Membr. Sci. 441 (2013) 45-53, 10.1016/j.memsci.2013.03.056.
[83] H. Nagasawa, Y. Yamamoto, N. Tsuda, M. Kanezashi, T. Yoshioka, T. Tsuru. Atmospheric-pressure plasma-enhanced chemical vapor deposition of microporous silica membranes for gas separation. J. Membr. Sci. 524 (2017) 644-651, 10.1016/j.memsci.2016.11.067.
[84] H. Nagasawa, T. Minamizawa, M. Kanezashi, T. Yoshioka, T. Tsuru. Microporous organosilica membranes for gas separation prepared via PECVD using different O/Si ratio precursors. J. Membr. Sci. 489 (2015) 11-19, 10.1016/j.memsci.2015.04.011.
[85] P. H. T. Ngamou, J. P. Overbeek, R. Kreiter, H. M. van Veen, J. F. Vente, I. M. Wienk, P. F. Cuperus, M. Creatore. Plasma-deposited hybrid silica membranes with a controlled retention of organic bridges. J. Mater. Chem. A. 1 (2013) 5567-5576, 10.1039/C3TA00120B.
[86] H. Nagasawa, T. Kagawa, T. Noborio, M. Kanezashi, A. Ogata, T. Tsuru. Ultrafast synthesis of silica-based molecular sieve membranes in dielectricbarrier discharge at low temperature and atmospheric pressure. J. Am. Chem. Soc. 143 (2021) 35-40, 10.1021/jacs.0c09433.
[87] N. Bighane, W. J. Koros. Novel silica membranes for high temperature gas separations. J. Membr. Sci. 371 (2011) 254-262, 10.1016/j.memsci.2011.01.045.

[88] J. Adams, N. Bighane, W. J. Koros. Pore morphology and temperature dependence of gas transport properties of silica membranes derived from oxidative thermolysis of polydimethylsiloxane. J. Membr. Sci. 524 (2017) 585-595, 10.1016/j.memsci.2016.11.074.
[89] S. Battersby, T. Tasaki, S. Smart, B. Ladewig, S. Liu, M. C. Duke, V. Rudolph, J. C. D. da Costa. Performance of cobalt silica membranes in gas mixture separation. J. Membr. Sci. 329 (2009) 91-98, 10.1016/j.memsci.2008.12.051.
[90] L. Yu, M. Kanezashi, H. Nagasawa, T. Tsuru. Fabrication and CO_2 permeation properties of amine-silica membranes using a variety of amine types. J. Membr. Sci. 541 (2017) 447-456, 10.1016/j.memsci.2017.07.024.
[91] M. Guo, J. Qian, R. Xu, X. Ren, J. Zhong, M. Kanezashi. Boosting the CO_2 capture efficiency through aromatic bridged organosilica membranes. J. Membr. Sci. 643 (2022) 120018, 10.1016/j.memsci.2021.120018.
[92] M. Guo, M. Kanezashi, H. Nagasawa, L. Yu, K. Yamamoto, T. Gunji, J. Ohshita, T. Tsuru. Tailoring the microstructure and permeation properties of bridged organosilica membranes via control of the bond angles. J. Membr. Sci. 584 (2019) 56-65, 10.1016/j.memsci.2019.04.072.
[93] M. Kanezashi, Y. Yoneda, H. Nagasawa, T. Tsuru, K. Yamamoto, J. Ohshita. Gas permeation properties for organosilica membranes with different Si/C ratios and evaluation of microporous structures. AIChE J. 63 (2017) 4491-4498, 10.1002/aic.15778.
[94] H. Song, Y. Wei, H. Qi. Tailoring pore structures to improve the permselectivity of organosilica membranes by tuning calcination parameters. J. Mater. Chem. A. 5 (2017) 24657-24666, 10.1039/c7ta07117e.
[95] S. Suzuki, S. B. Messaoud, A. Takagaki, T. Sugawara, R. Kikuchi, S. T. Oyama. Development of inorganic–organic hybrid membranes for carbon dioxide/methane separation. J. Membr. Sci. 471 (2014) 402-411, 10.1016/j.memsci.2014.08.029.
[96] L. Yu, M. Kanezashi, H. Nagasawa, M. Guo, N. Moriyama, K. Ito, T. Tsuru. Tailoring ultramicroporosity to maximize CO_2 transport within pyrimidine-bridged organosilica membranes. ACS Appl. Mater. Interfaces. 11 (2019) 7164-7173, 10.1021/acsami.9b01462.
[97] H. Nagasawa, T. Niimi, M. Kanezashi, T. Yoshioka, T. Tsuru. Modified gas-translation model for prediction of gas permeation through microporous organosilica membranes. AIChE J. 60 (2014) 4199-4210, 10.1002/aic.14578.
[98] H. R. Lee, M. Kanezashi, Y. Shimomura, T. Yoshioka, T. Tsuru. Evaluation and fabrication of pore-size-tuned silica membranes with tetraethoxydimethyl disiloxane for gas separation. AIChE J. 57 (2011) 2755-2765, 10.1002/aic.12501.
[99] J. Xiao, J. Wei. Diffusion mechanism of hydrocarbons in zeolites—I. Theory. Chem. Eng. Sci. 47 (1992) 1123-1141, 10.1016/0009-2509(92)80236-6.
[100] B. Yao, S. Mandra, J. O. Curry, S. Shaikhutdinov, H. J. Freund, J. Schrier. Gas separation through bilayer silica, the thinnest possible silica membrane. ACS Appl. Mater. Interfaces. 9 (2017) 43061-43071, 10.1021/acsami.7b13302.
[101] T. Yoshioka, M. Kanezashi, T. Tsuru. Micropore size estimation on gas separation membranes: A study in experimental and molecular dynamics. AIChE J. 59 (2013) 2179-2194, 10.1002/aic.13966.
[102] K. Yamamoto, S. Koge, K. Sasahara, T. Mizumo, Y. Kaneko, M. Kanezashi, T. Tsuru, J. Ohshita. Preparation of bridged polysilsesquioxane membranes from bis[3-

(triethoxysilyl)propyl]amine for water desalination. Bull. Chem. Soc. Jpn. 90 (2017) 1035-1040, 10.1246/bcsj.20170153.
[103] T. Yoshioka, M. Asaeda, T. Tsuru. A molecular dynamics simulation of pressure-driven gas permeation in a micropore potential field on silica membranes. J. Membr. Sci. 293 (2007) 81-93, 10.1016/j.memsci.2007.01.039.
[104] P. Sahu, S. M. Ali. An atomistic perspective on the diffusion and permeation of hydrogen and isotopes through an engineered nanoporous silica membrane using molecular dynamics simulations. Mol. Syst. Des. Eng. 7 (2022) 1501-1515, 10.1039/D2ME00041E.
[105] T. Yoshioka, A. Nakata, K.-L. Tung, M. Kanezashi, T. Tsuru. Molecular dynamics simulation study of solid vibration permeation in microporous amorphous silica network voids. Membranes. 9 (2019) 132, 10.3390/membranes9100132.
[106] K.-S. Chang, T. Yoshioka, M. Kanezashi, T. Tsuru, K.-L. Tung. Molecular simulation of micro-structures and gas diffusion behavior of organic–inorganic hybrid amorphous silica membranes. J. Membr. Sci. 381 (2011) 90-101, 10.1016/j.memsci.2011.07.020.
[107] K.-S. Chang, T. Yoshioka, M. Kanezashi, T. Tsuru, K.-L. Tung. A molecular dynamics simulation of a homogeneous organic–inorganic hybrid silica membrane. ChemComm. 46 (2010) 9140-9142, 10.1039/C0CC02531C.
[108] A. I. Labropoulos, G. E. Romanos, G. N. Karanikolos, F. K. Katsaros, N. K. Kakizis, N. K. Kanellopoulos. Comparative study of the rate and locality of silica deposition during the CVD treatment of porous membranes with TEOS and TMOS. Microporous Mesoporous Mater. 120 (2009) 177-185, 10.1016/j.micromeso.2008.08.063.
[109] S.-i. Nakao, T. Suzuki, T. Sugawara, T. Tsuru, S. Kimura. Preparation of microporous membranes by TEOS/O_3 CVD in the opposing reactants geometry. Microporous Mesoporous Mater. 37 (2000) 145-152, 10.1016/S1387-1811(99)00261-9.
[110] M. Nomura, T. Yamaguchi, S.-i. Nakao. Silicalite membranes modified by counterdiffusion CVD technique. Ind. Eng. Chem. Res. 36 (1997) 4217-4223, 10.1021/ie970338a.
[111] T. Yamaguchi, X. Ying, Y. Tokimasa, B. N. Nair, T. Sugawara, S.-i. Nakao. Reaction control of tetraethyl orthosilicate (TEOS)/O_3 and tetramethyl orthosilicate (TMOS)/O_3 counter diffusion chemical vapour deposition for preparation of molecular-sieve membranes. Phys. Chem. Chem. Phys. 2 (2000) 4465-4469, 10.1039/B004642F.
[112] M. Nomura, K. Ono, S. Gopalakrishnan, T. Sugawara, S.-I. Nakao. Preparation of a stable silica membrane by a counter diffusion chemical vapor deposition method. J. Membr. Sci. 251 (2005) 151-158, 10.1016/j.memsci.2004.11.008.
[113] H.-S. Choi, C.-H. Ryu, G.-J. Hwang. Materials Advances. Chem. Eng. J. 232 (2013) 302-309, 10.1016/j.cej.2013.07.105.
[114] J. Yu, H.-K. Lim, S. Lee. Transition-metal softener for high-durability hydrogen separation silica membranes. J. Phys. Chem. C. 123 (2019) 25761-25768, 10.1021/acs.jpcc.9b08068.
[115] S.-J. Ahn, G.-N. Yun, A. Takagaki, R. Kikuchi, S. T. Oyama. Synthesis and characterization of hydrogen selective silica membranes prepared by chemical vapor deposition of vinyltriethoxysilane. J. Membr. Sci. 550 (2018) 1-8, 10.1016/j.memsci.2017.12.038.
[116] Y. Gu, P. Hacarlioglu, S. T. Oyama. Hydrothermally stable silica–alumina composite membranes for hydrogen separation. J. Membr. Sci. 310 (2008) 28-37, 10.1016/j.memsci.2007.10.025.

[117] R. Igi, T. Yoshioka, Y. H. Ikuhara, Y. Iwamoto, T. Tsuru. Characterization of Co-doped silica for improved hydrothermal stability and application to hydrogen separation membranes at high temperatures. J. Am. Ceram. Soc. 91 (2008) 2975-2981, 10.1111/j.1551-2916.2008.02563.x.
[118] S. M. Ibrahim, H. Nagasawa, M. Kanezashi, T. Tsuru. Robust organosilica membranes for high temperature reverse osmosis (RO) application: Membrane preparation, separation characteristics of solutes and membrane regeneration. J. Membr. Sci. 493 (2015) 515-523, 10.1016/j.memsci.2015.06.060.
[119] G. Gong, H. Nagasawa, M. Kanezashi, T. Tsuru. Reverse osmosis performance of layered-hybrid membranes consisting of an organosilica separation layer on polymer supports. J. Membr. Sci. 494 (2015) 104-112, 10.1016/j.memsci.2015.07.039.
[120] S. M. Ibrahim, H. Nagasawa, M. Kanezashi, T. Tsuru. Organosilica bis (triethoxysilyl) ethane (BTESE) membranes for gas permeation (GS) and reverse osmosis (RO): The effect of preparation conditions on structure, and the correlation between gas and liquid permeation properties. J. Membr. Sci. 526 (2017) 242-251, 10.1016/j.memsci.2016.12.036.
[121] S. M. Ibrahim, H. Nagasawa, M. Kanezashi, T. Tsuru. Chemical-free cleaning of fouled reverse osmosis (RO) membranes derived from bis (triethoxysilyl) ethane (BTESE). J. Membr. Sci. 601 (2020) 117919, 10.1016/j.memsci.2020.117919.
[122] H. L. Castricum, A. Sah, R. Kreiter, D. H. A. Blank, J. F. Vente, J. E. ten Elshof. Hydrothermally stable molecular separation membranes from organically linked silica. J. Mater. Chem. 18 (2008) 2150-2158, 10.1039/b801972j.
[123] R. Xu, J. Wang, M. Kanezashi, T. Yoshioka, T. Tsuru. Reverse osmosis performance of organosilica membranes and comparison with the pervaporation and gas permeation properties. AIChE J. 59 (2013) 1298-1307, 10.1002/aic.13885.
[124] N. Moriyama, H. Nagasawa, M. Kanezashi, T. Tsuru. Selective water vapor permeation from steam/non-condensable gas mixtures via organosilica membranes at moderate-to-high temperatures. J. Membr. Sci. 589 (2019) 117254, 10.1016/j.memsci.2019.117254.
[125] L. Yu, M. Kanezashi, H. Nagasawa, J. Oshita, A. Naka, T. Tsuru. Pyrimidine-bridged organoalkoxysilane membrane for high-efficiency CO_2 transport via mild affinity. Sep. Purif. Technol. 178 (2017) 232-241, 10.1016/j.seppur.2017.01.039.
[126] M. Kanezashi, T. Matsutani, T. Wakihara, H. Nagasawa, T. Okubo, T. Tsuru. Preparation and gas permeation properties of fluorine–silica membranes with controlled amorphous silica structures: effect of fluorine source and calcination temperature on network size. ACS Appl. Mater. Interfaces. 9 (2017) 24625-24633, 10.1021/acsami.7b06800.
[127] M. Kanezashi, S. Miyauchi, H. Nagasawa, T. Yoshioka, T. Tsuru. Gas permeation properties through Al-doped organosilica membranes with controlled network size. J. Membr. Sci. 466 (2014) 246-252, 10.1016/j.memsci.2014.04.051.
[128] M. Kanezashi, W. Shazwani, T. Yoshioka, T. Tsuru. Separation of propylene/propane binary mixtures by bis (triethoxysilyl) methane (BTESM)-derived silica membranes fabricated at different calcination temperatures. J. Membr. Sci. 415 (2012) 478-485, 10.1016/j.memsci.2012.05.034.
[129] K. Yamamoto, H. Muragishi, T. Mizumo, T. Gunji, M. Kanezashi, T. Tsuru, J. Ohshita. Diethylenedioxane-bridged microporous organosilica membrane for gas and water separation. Sep. Purif. Technol. 207 (2018) 370-376, 10.1016/j.seppur.2018.06.036.

[130] J. Ohshita, H. Muragishi, K. Yamamoto, T. Mizumo, M. Kanezashi, T. Tsuru. Preparation and separation properties of porous norbornane-bridged silica membrane. J. Solgel Sci. Technol. 73 (2015) 365-370, 10.1007/s10971-014-3542-y.
[131] T. Mizumo, H. Muragishi, K. Yamamoto, J. Ohshita, M. Kanezashi, T. Tsuru. Preparation and separation properties of oxalylurea-bridged silica membranes. Appl. Organomet. Chem. 29 (2015) 433-438, 10.1002/aoc.3311.
[132] X.-L. Zhang, H. Yamada, T. Saito, T. Kai, K. Murakami, M. Nakashima, J. Ohshita, K. Akamatsu, S.-i. Nakao. Development of hydrogen-selective triphenylmethoxysilane-derived silica membranes with tailored pore size by chemical vapor deposition. J. Membr. Sci. 499 (2016) 28-35, 10.1016/j.memsci.2015.09.025.
[133] V. Boffa, D. Blank, J. Tenelshof. Hydrothermal stability of microporous silica and niobia–silica membranes. J. Membr. Sci. 319 (2008) 256-263, 10.1016/j.memsci.2008.03.042.
[134] M. Kanezashi, D. Fuchigami, T. Yoshioka, T. Tsuru. Control of Pd dispersion in sol–gel-derived amorphous silica membranes for hydrogen separation at high temperatures. J. Membr. Sci. 439 (2013) 78-86, 10.1016/j.memsci.2013.03.037.
[135] E. Ş. Mirza, B. Topuz. Nanoscale tailoring on thin bimetallic organo-oxide membranes for H_2/CO_2 separation. Sep. Purif. Technol. 280 (2022) 119801, 10.1016/j.seppur.2021.119801.
[136] H. Qi, J. Han, N. Xu. Effect of calcination temperature on carbon dioxide separation properties of a novel microporous hybrid silica membrane. J. Membr. Sci. 382 (2011) 231-237, 10.1016/j.memsci.2011.08.013.
[137] H. Song, S. Zhao, J. Lei, C. Wang, H. Qi. Pd-doped organosilica membrane with enhanced gas permeability and hydrothermal stability for gas separation. J. Mater. Sci. 51 (2016) 6275-6286, 10.1007/s10853-016-9924-5.
[138] M. ten Hove, A. Nijmeijer, L. Winnubst. Facile synthesis of zirconia doped hybrid organic inorganic silica membranes. Sep. Purif. Technol. 147 (2015) 372-378, 10.1016/j.seppur.2014.12.033.
[139] H. Song, S. Zhao, J. Chen, H. Qi. Hydrothermally stable Zr-doped organosilica membranes for H_2/CO_2 separation. Microporous Mesoporous Mater. 224 (2016) 277-284, 10.1016/j.micromeso.2016.01.001.
[140] H. Qi, H. Chen, L. Li, G. Zhu, N. Xu. Effect of Nb content on hydrothermal stability of a novel ethylene-bridged silsesquioxane molecular sieving membrane for H_2/CO_2 separation. J. Membr. Sci. 421-422 (2012) 190-200, 10.1016/j.memsci.2012.07.010.
[141] P. Karakiliç, C. Huiskes, M. W. J. Luiten-Olieman, A. Nijmeijer, L. Winnubst. Sol-gel processed magnesium-doped silica membranes with improved H_2/CO_2 separation. J. Membr. Sci. 543 (2017) 195-201, 10.1016/j.memsci.2017.08.055.
[142] J. Yang, W. Fan, C.-M. Bell. Effect of calcination atmosphere on microstructure and H_2/CO_2 separation of palladium-doped silica membranes. Sep. Purif. Technol. 210 (2019) 659-669, 10.1016/j.seppur.2018.08.041.
[143] H.-F. Zhang, W. Liu, J.-J. Lei. Pd doping on H_2/CO_2 separation performance and hydrothermal stability of organic-inorganic hybrid SiO_2 membranes. Inorg. Mater. 33 (2018) 1316-1322, 10.15541/jim20180189.
[144] Q. Jiang, M. Guo. Network structure engineering of organosilica membranes for enhanced CO_2 capture performance. Membranes. 12 (2022) 470, 10.3390/membranes12050470.

[145] M. Guo, M. Kanezashi, H. Nagasawa, L. Yu, J. Ohshita, T. Tsuru. Amino-decorated organosilica membranes for highly permeable CO_2 capture. J. Membr. Sci. 611 (2020) 118328, 10.1016/j.memsci.2020.118328.
[146] S. Chai, H. Du, Y. Zhao, Y. Lin, C. Kong, L. Chen. Fabrication of highly selective organosilica membrane for gas separation by mixing bis(triethoxysilyl)ethane with methyltriethoxysilane. Sep. Purif. Technol. 222 (2019) 162-167, 10.1016/j.seppur.2019.04.039.
[147] M. Guo, Y. Zhang, R. Xu, X. Ren, W. Huang, J. Zhong, T. Tsuru, M. Kanezashi. Ultrahigh permeation of CO_2 capture using composite organosilica membranes. Sep. Purif. Technol. 282 (2022) 120061, 10.1016/j.seppur.2021.120061.
[148] I. Rana, H. Nagasawa, T. Tsuru, M. Kanezashi. Tailoring the structure of a sub-nano silica network via fluorine doping to enhance CO_2 separation and evaluating CO_2 separation performance under dry or wet conditions. J. Membr. Sci. 658 (2022) 120735, 10.1016/j.memsci.2022.120735.
[149] A. P. Dral, E. Johan. Organic groups influencing microporosity in organosilicas. Microporous Mesoporous Mater. 267 (2018) 267-273, 10.1016/j.micromeso.2018.03.036.
[150] M. Takenaka, H. Nagasawa, T. Tsuru, M. Kanezashi. Hydrocarbon permeation properties through microporous fluorine-doped organosilica membranes with controlled pore sizes. J. Membr. Sci. 619 (2021) 118787, 10.1016/j.memsci.2020.118787.
[151] L. Yu, M. Kanezashi, H. Nagasawa, J. Ohshita, A. Naka, T. Tsuru. Fabrication and microstructure tuning of a pyrimidine-bridged organoalkoxysilane membrane for CO_2 separation. Ind. Eng. Chem. Res. 56 (2017) 1316-1326, 10.1021/acs.iecr.6b04460.
[152] Y. Mise, S. J. Ahn, A. Takagaki, R. Kikuchi, S. T. Oyama. Fabrication and evaluation of trimethylmethoxysilane (TMMOS)-derived membranes for gas separation. Membranes 9(2019) 123, 10.3390/membranes9100123.
[153] M. Kanezashi, M. Asaeda. Hydrogen permeation characteristics and stability of Ni-doped silica membranes in steam at high temperature. J. Membr. Sci. 271 (2006) 86-93, 10.1016/j.memsci.2005.07.011.
[154] Y. Zhao, C. Zhou, C. Kong, L. Chen. Ultrathin reduced graphene oxide/organosilica hybrid membrane for gas separation. JACS Au. 1 (2021) 328-335, 10.1021/jacsau.0c00073.
[155] D. He, H. Zhang, Y. Ren, H. Qi. Fabrication of a novel microporous membrane based on ZIF-7 doped 1,2-bis(triethoxysilyl)ethane for H_2/CO_2 separation. Microporous Mesoporous Mater. 331 (2022) 111674, 10.1016/j.micromeso.2021.111674.
[156] C. Kong, H. Du, L. Chen, B. Chen. Nanoscale MOF/organosilica membranes on tubular ceramic substrates for highly selective gas separation. Energy Environ. Sci. 10 (2017) 1812-1819, 10.1039/c7ee00830a.
[157] L. Meng, M. Kanezashi, J. Wang, T. Tsuru. Permeation properties of BTESE–TEOS organosilica membranes and application to O_2/SO_2 gas separation. J. Membr. Sci. 496 (2015) 211-218, 10.1016/j.memsci.2015.08.066.
[158] H. Zhang, D. He, S. Niu, H. Qi. Tuning the microstructure of organosilica membranes with improved gas permselectivity via the co-polymerization of 1,2-bis(triethoxysilyl)ethane and 1,2-bis(triethoxysilyl)methane. Int. J. Hydrog. Energy. 46 (2021) 17221-17230, 10.1016/j.ijhydene.2021.02.139.
[159] X. Ren, M. Kanezashi, H. Nagasawa, R. Xu, J. Zhong, T. Tsuru. Ceramic-supported polyhedral oligomeric silsesquioxane–organosilica nanocomposite membrane for

efficient gas separation. Ind. Eng. Chem. Res. 58 (2019) 21708-21716, 10.1021/acs.iecr.9b05251.
[160] X. Ren, M. Kanezashi, M. Guo, R. Xu, J. Zhong, T. Tsuru. Multiple amine-contained POSS-functionalized organosilica membranes for gas separation. Membranes. 11 (2021) 194, 10.3390/membranes11030194.
[161] J.-Y. Li, D. K. Wang, Y.-T. Lin, M.-Y. Wey, H.-H. Tseng. Homogeneous sub-nanophase network tailoring of dual organosilica membrane for enhancing CO_2 gas separation. J. Membr. Sci. 644 (2022) 120170, 10.1016/j.memsci.2021.120170.
[162] M. Guo, M. Kanezashi, H. Nagasawa, L. Yu, K. Yamamoto, T. Gunji, J. Ohshita, T. Tsuru. Pore subnano-environment engineering of organosilica membranes for highly selective propylene/propane separation. J. Membr. Sci. 603 (2020) 117999, 10.1016/j.memsci.2020.117999.
[163] A. M. Tandel, W. Guo, K. Bye, L. Huang, M. Galizia, H. Lin. Designing organic solvent separation membranes: polymers, porous structures, 2D materials, and their combinations. Mater. Adv. 2 (2021) 4574-4603, 10.1039/D1MA00373A.
[164] P. Marchetti, M. F. Jimenez Solomon, G. Szekely, A. G. Livingston. Molecular separation with organic solvent nanofiltration: A critical review. Chem. Rev. 114 (2014) 10735-10806, 10.1021/cr500006j.
[165] P. Boutikos, C. S. Pereira, V. M. Silva, A. E. Rodrigues. Performance evaluation of silica membrane for water–n-butanol binary mixture. Sep. Purif. Technol. 127 (2014) 18-28, 10.1016/j.seppur.2014.02.019.
[166] H. M. Van Veen, M. D. Rietkerk, D. P. Shanahan, M. M. Van Tuel, R. Kreiter, H. L. Castricum, E. Johan, J. F. Vente. Pushing membrane stability boundaries with HybSi® pervaporation membranes. J. Membr. Sci. 380 (2011) 124-131, 10.1016/j.memsci.2011.06.040.
[167] H. L. Castricum, G. G. Paradis, M. C. Mittelmeijer‐Hazeleger, R. Kreiter, J. F. Vente, J. E. Ten Elshof. Tailoring the separation behavior of hybrid organosilica membranes by adjusting the structure of the organic bridging group. Adv. Funct. Mater. 21 (2011) 2319-2329, 10.1002/adfm.201002361.
[168] R. Kreiter, M. D. Rietkerk, H. L. Castricum, H. M. van Veen, J. E. ten Elshof, J. F. Vente. Stable hybrid silica nanosieve membranes for the dehydration of lower alcohols. ChemSusChem. 2 (2009) 158-160, 10.1002/cssc.200800198.
[169] B. Bettens, S. Dekeyzer, B. Van der Bruggen, J. Degrève, C. Vandecasteele. Transport of pure components in pervaporation through a microporous silica membrane. J. Phys. Chem. B. 109 (2005) 5216-5222, 10.1021/jp044515e.
[170] C. Casado, A. Urtiaga, D. Gorri, I. Ortiz. Pervaporative dehydration of organic mixtures using a commercial silica membrane: Determination of kinetic parameters. Sep. Purif. Technol. 42 (2005) 39-45, 10.1016/j.seppur.2004.06.002.
[171] S. Sommer, B. Klinkhammer, T. Melin. Integrated system design for dewatering of solvents with microporous silica membranes. Desalination. 149 (2002) 15-21, 10.1016/S0011-9164(02)00685-9.
[172] S. Sommer, T. Melin. Influence of operation parameters on the separation of mixtures by pervaporation and vapor permeation with inorganic membranes. Part 1: Dehydration of solvents. Chem. Eng. Sci. 60 (2005) 4509-4523, 10.1016/j.ces.2005.02.059.

[173] W. Raza, J. Yang, J. Wang, H. Saulat, G. He, J. Lu, Y. Zhang. HCl modification and pervaporation performance of BTESE membrane for the dehydration of acetic acid/water mixture. Sep. Purif. Technol. 235 (2020) 116102, 10.1016/j.seppur.2019.116102.
[174] M. Asaeda, J. Yang, Y. Sakou. Porous silica-zirconia (50%) membranes for pervaporation of iso-propyl alcohol (IPA)/Water mixtures. J. Chem. Eng. Japan. 35 (2002) 365-371, 10.1252/jcej.35.365.
[175] J. Wang, T. Tsuru. Cobalt-doped silica membranes for pervaporation dehydration of ethanol/water solutions. J. Membr. Sci. 369 (2011) 13-19, 10.1016/j.memsci.2010.10.062.
[176] T. Tsuru, T. Shibata, J. Wang, H. R. Lee, M. Kanezashi, T. Yoshioka. Pervaporation of acetic acid aqueous solutions by organosilica membranes. J. Membr. Sci. 421 (2012) 25-31, 10.1016/j.memsci.2012.06.012.
[177] X. Lu, M. Elimelech. Fabrication of desalination membranes by interfacial polymerization: history, current efforts, and future directions. Chem. Soc. Rev. 50 (2021) 6290-6307, 10.1039/D0CS00502A.
[178] Z. Yang, X.-H. Ma, C. Y. Tang. Recent development of novel membranes for desalination. Desalination. 434 (2018) 37-59, 10.1016/j.desal.2017.11.046.
[179] P. Goh, W. Lau, M. Othman, A. Ismail. Membrane fouling in desalination and its mitigation strategies. Desalination. 425 (2018) 130-155, 10.1016/j.desal.2017.10.018.
[180] S. Avlonitis, K. Kouroumbas, N. Vlachakis. Energy consumption and membrane replacement cost for seawater RO desalination plants. Desalination. 157 (2003) 151-158, 10.1016/S0011-9164(03)00395-3.
[181] M. Elma, D. K. Wang, C. Yacou, J. C. Diniz da Costa. Interlayer-free P123 carbonised template silica membranes for desalination with reduced salt concentration polarisation. J. Membr. Sci. 475 (2015) 376-383, 10.1016/j.memsci.2014.10.026.
[182] R. Xu, J. Wang, M. Kanezashi, T. Yoshioka, T. Tsuru. Development of robust organosilica membranes for reverse osmosis. Langmuir. 27 (2011) 13996-13999, 10.1021/la203711u.
[183] K. Yamamoto, J. Ohshita, T. Mizumo, M. Kanezashi, T. Tsuru. Synthesis of organically bridged trialkoxysilanes bearing acetoxymethyl groups and applications to reverse osmosis membranes. Appl. Organomet. Chem. 31 (2017) e3580, 10.1002/aoc.3580.
[184] R. Xu, S. M. Ibrahim, M. Kanezashi, T. Yoshioka, K. Ito, J. Ohshita, T. Tsuru. New insights into the microstructure-separation properties of organosilica membranes with ethane, ethylene, and acetylene bridges. ACS Appl. Mater. Interfaces. 6 (2014) 9357-9364, 10.1021/am501731d.
[185] D. Zhang, M. Kanezashi, T. Tsuru, K. Yamamoto, T. Gunji, Y. Adachi, J. Ohshita. Development of PSQ-RO membranes with high water permeability by copolymerization of bis[3-(triethoxysilyl)propyl]amine and triethoxy(3-glycidyloxypropyl)silane. J. Membr. Sci. 644 (2022) 120162, 10.1016/j.memsci.2021.120162.
[186] F.-T. Zheng, K. Yamamoto, M. Kanezashi, T. Tsuru, J. Ohshita. Preparation of bridged silica RO membranes from copolymerization of bis(triethoxysilyl)ethene/(hydroxymethyl)triethoxysilane. Effects of ethenylene-bridge enhancing water permeability. J. Membr. Sci. 546 (2018) 173-178, 10.1016/j.memsci.2017.10.025.
[187] R. Lestari, M. Elma, A. Rahma, D. Suparsih, S. Anadhliyah, N. Ledyana, D. Pratomo, A. Sumardi, A. Lestari, Z. Assyaifi, G. Satriaji. Organo silica membranes for wetland saline

water desalination: effect of membranes calcination temperatures. E3S Web Conf. 148 (2020) 07006, 10.1051/e3sconf/202014807006.
[188] S. Wang, D. K. Wang, J. Motuzas, S. Smart, J. C. Diniz da Costa. Rapid thermal treatment of interlayer-free ethyl silicate 40 derived membranes for desalination. J. Membr. Sci. 516 (2016) 94-103, 10.1016/j.memsci.2016.06.005.
[189] R. Xu, Q. Liu, X. Ren, P. Lin, J. Zhong. Tuning the pore structures of organosilica membranes for enhanced desalination performance via the control of calcination temperatures. Membranes. 10 (2020) 392, 10.3390/membranes10120392.
[190] R. Xu, P. Lin, Q. Zhang, J. Zhong, T. Tsuru. Development of ethenylene-bridged organosilica membranes for desalination applications. Ind. Eng. Chem. Res. 55 (2016) 2183-2190, 10.1021/acs.iecr.5b04439.
[191] C. X. C. Lin, L. P. Ding, S. Smart, J. C. Diniz da Costa. Cobalt oxide silica membranes for desalination. J. Colloid Interface Sci. 368 (2012) 70-76, 10.1016/j.jcis.2011.10.041.
[192] A. Darmawan, L. Karlina, Y. Astuti, Sriatun, J. Motuzas, D. K. Wang, J. C. D. da Costa. Structural evolution of nickel oxide silica sol-gel for the preparation of interlayer-free membranes. J. Non-Cryst. Solids. 447 (2016) 9-15, 10.1016/j.jnoncrysol.2016.05.031.
[193] H.-Y. Zhang, J.-L. Wen, Q. Shao, A. Yuan, H.-T. Ren, F.-Y. Luo, X.-L. Zhang. Fabrication of La/Y-codoped microporous organosilica membranes for high-performance pervaporation desalination. J. Membr. Sci. 584 (2019) 353-363, 10.1016/j.memsci.2019.05.023.
[194] M. Elma, D. R. Mujiyanti, N. M. Ismail, M. R. Bilad, A. Rahma, S. K. Rahman, Fitriani, A. Rakhman, E. L. A. Rampun. Development of hybrid and templated silica-P123 membranes for brackish water desalination. Polymers. 12 (2020), 10.3390/polym12112644.
[195] H. Yang, D. K. Wang, J. Motuzas, J. C. Diniz da Costa. Hybrid vinyl silane and P123 template sol−gel derived carbon silica membrane for desalination. J. Solgel Sci. Technol. 85 (2018) 280-289, 10.1007/s10971-017-4562-1.
[196] H. Yang, M. Elma, D. K. Wang, J. Motuzas, J. C. D. da Costa. Interlayer-free hybrid carbon-silica membranes for processing brackish to brine salt solutions by pervaporation. J. Membr. Sci. 523 (2017) 197-204.
[197] B. P. Ladewig, Y. H. Tan, C. X. C. Lin, K. Ladewig, J. C. Diniz da Costa, S. Smart. Preparation, characterization and performance of templated silica membranes in non-osmotic desalination. Materials. 4 (2011) 845-856, 10.3390/ma4040845.
[198] D. R. Mujiyanti, M. Elma, M. Amalia. Interlayer-free glucose carbonised template silica membranes for brine water desalination. MATEC Web Conf. 280 (2019) 03010, 10.1051/matecconf/201928003010.
[199] F. R. Mustalifah, A. Rahma, Mahmud, Sunardi, M. Elma. Chemical cleaning to evaluate the performance of silica-pectin membrane on acid mine drainage desalination. IOP Conf. Ser.: Mater. Sci. Eng. 1195 (2021) 012057, 10.1088/1757-899x/1195/1/012057.
[200] M. C. Duke, S. Mee, J. C. D. da Costa. Performance of porous inorganic membranes in non-osmotic desalination. Water Res. 41 (2007) 3998-4004, 10.1016/j.watres.2007.05.028.
[201] G. Dong, H. Nagasawa, L. Yu, Q. Wang, K. Yamamoto, J. Ohshita, M. Kanezashi, T. Tsuru. Pervaporation removal of methanol from methanol/organic azeotropes using organosilica membranes: Experimental and modeling. J. Membr. Sci. 610 (2020) 118284, 10.1016/j.memsci.2020.118284.

[202] T. Sato, H. Nagasawa, M. Kanezashi, T. Tsuru. Enhanced production of butyl acetate via methanol-extracting transesterification membrane reactors using organosilica membrane: Experiment and modeling. Chem. Eng. J. 429 (2022) 132188, 10.1016/j.cej.2021.132188.
[203] T. Sato, H. Nagasawa, M. Kanezashi, T. Tsuru. Transesterification membrane reactor with organosilica membrane in batch and continuous flow modes. Chem. Eng. J. 450 (2022) 137862, 10.1016/j.cej.2022.137862.
[204] G. Dong, Y. Zhang, T. Sato, H. Nagasawa, M. Kanezashi, T. Tsuru. Reverse osmosis and pervaporation of organic liquids using organosilica membranes: Performance analysis and predictions. AIChE J. 68 (2022) e17585, 10.1002/aic.17585.
[205] V. M. Silva, C. S. Pereira, A. E. Rodrigues. PermSMBR—A new hybrid technology: Application on green solvent and biofuel production. AIChE J. 57 (2011) 1840-1851.
[206] C. S. Pereira, V. M. Silva, S. P. Pinho, A. E. Rodrigues. Batch and continuous studies for ethyl lactate synthesis in a pervaporation membrane reactor. J. Membr. Sci. 361 (2010) 43-55, 10.1016/j.memsci.2010.06.014.
[207] H. F. Collazos, J. Fontalvo, M. Á. Gómez-García. Design directions for ethyl lactate synthesis in a pervaporation membrane reactor. Desalin. Water Treat. 51 (2013) 2394-2401, 10.1080/19443994.2012.728069.
[208] D. S. Constantino, R. P. Faria, A. E. Rodrigues. Sorption-enhanced reaction with simulated moving bed reactor and PermSMBR technologies. Advances in Chemical Engineering: Elsevier; 2017. p. 261-330.
[209] N. Kageyama, A. Takagaki, T. Sugawara, R. Kikuchi, S. T. Oyama. Synthesis and characterization of a silica-alumina composite membrane and its application in a membrane reactor. Sep. Purif. Technol. 195 (2018) 437-445, 10.1016/j.seppur.2017.12.021.
[210] R. Nishida, T. Tago, T. Saitoh, M. Seshimo, S. I. Nakao. Development of CVD silica membranes having high hydrogen permeance and steam durability and a membrane reactor for a water gas shift reaction. Membranes. 9 (2019), 10.3390/membranes9110140.
[211] K. Ghasemzadeh, A. Aghaeinejad-Meybodi, M. J. Vaezi, A. Gholizadeh, M. A. Abdi, A. A. Babaluo, M. Haghighi, A. Basile. Hydrogen production via silica membrane reactor during the methanol steam reforming process: experimental study. RSC Adv. 5 (2015) 95823-95832, 10.1039/C5RA14002A.
[212] O. Myagmarjav, N. Tanaka, M. Nomura, S. Kubo. Module design of silica membrane reactor for hydrogen production via thermochemical IS process. Int. J. Hydrog. Energy. 44 (2019) 10207-10217, 10.1016/j.ijhydene.2019.02.192.
[213] O. Myagmarjav, N. Tanaka, M. Nomura, H. Noguchi, Y. Imai, Y. Kamiji, S. Kubo, H. Takegami. Development of a membrane reactor with a closed-end silica membrane for nuclear-heated hydrogen production. Prog. Nucl. Energy. 137 (2021) 103772, 10.1016/j.pnucene.2021.103772.
[214] M. Seshimo, H. Urai, K. Sasa, H. Nishino, Y. Yamaguchi, R. Nishida, S.-i. Nakao. Bench-scale membrane reactor for methylcyclohexane dehydrogenation using silica membrane module. Membranes. 11 (2021), 10.3390/membranes11050326.
[215] L. Meng, X. Yu, T. Niimi, H. Nagasawa, M. Kanezashi, T. Yoshioka, T. Tsuru. Methylcyclohexane dehydrogenation for hydrogen production via a bimodal catalytic membrane reactor. AIChE J. 61 (2015) 1628-1638, 10.1002/aic.14764.